Bulletin of the JSME Vol.10, No.6, 2023
Mechanical Engineering Journal

Substructure elimination method for evaluating bending vibration of beams

Keisuke YAMADA* and Jinchen JI**
*Faculty of Engineering Science, Kansai University
3-3-35 Yamate-cho, Suita-shi, Osaka 564-8680, Japan
E-mail: yamadak@kansai-u.ac.jp
**School of Mechanical and Mechatronic Engineering, University of Technology Sydney
Ultimo, NSW 2007, Australia

Received: 25 July 2023; Revised: 25 September 2023; Accepted: 4 October 2023

Abstract
In this study, a vibration analysis method is presented based on the substructure elimination method for a Bernoulli-Euler beam. Vibration analysis using modal analysis is effective for reducing the degrees of freedom and enables the analysis of a beam on which actuators and sensors are installed. When mechanical impedances are installed at the boundaries or the beam is coupled to other structures, a free-free beam is employed for conventional modal analysis using continuous functions. However, conventional modal analysis provides inaccurate simulation results when the coupled mechanical impedances considering the characteristic impedances of the beam are large. To address this issue, the modal analysis of a beam using the substructure elimination method was proposed in this study. Because the substructure elimination method for beams was only briefly reported on by the first author, several problems currently exist. To solve these problems, a substructure elimination method is proposed using a simply supported beam in addition to a guided-guided beam. Additionally, a new formulation method based on constraint conditions was proposed as a versatile method for setting arbitrary boundary conditions. The appropriate length, line density, and bending stiffness of the elimination regions, and the highest order of the eigenmode, were determined through simulations. The effectiveness of the proposed method was then verified by comparing the simulation results of the proposed method and exact solutions obtained using the boundary conditions. Based on a comparison with the simulation results of conventional modal analysis using a free-free beam, the precision of the proposed method is significantly higher than that of conventional modal analysis.

Keywords : Bernoulli-Euler beam, Bending vibration, Modal analysis, Coupled vibration, Continuum vibration, Simulation, Displacement excitation, Non-reflective boundary

1. Introduction

The development of vibration simulation technology has reduced the amount of equipment used in prototyping. Vibration simulation technology is particularly supported by the finite element method (FEM), which allows for the vibration simulation of machines with complex shapes. Currently, although it is possible to simulate the vibration of complex shapes, it is also important to capture the essence of the vibration phenomenon in a simpler way during early design stages. In this regard, one-dimensional computer-aided engineering (1D CAE) is also attracting attention (Ohtomi, 2015). Although 1D CAE is not explicitly applied one-dimensionally, the focus in this study is developing a vibration analysis method for a one-dimensional continuous body, assuming that it will be used in basic research and 1D CAE. The one-dimensional continuous bodies that are of particular importance in vibration engineering are beams and acoustic fields in ducts. The equations of motion for the beam and acoustic field are expressed using a fourth-order partial differential equation and wave equation, respectively. Because these equations differ significantly, the continuous bodies governed by a one-dimensional wave equation was described in a previous study (Yamada and Ji, 2023). Therefore, the vibration analysis method for Bernoulli-Euler beams is described here.

Paper No.23-00293
J-STAGE Advance Publication date : 14 October, 2023
[DOI: 10.1299/mej.23-00293]

© 2023 The Japan Society of Mechanical Engineers. This is an open access article under the terms of the Creative Commons Attribution-NonCommercial-NoDerivs license (https://creativecommons.org/licenses/by-nc-nd/4.0/).

FEM can be used to analyze the vibration of a beam. However, FEM has the disadvantage that it requires the discretization of the beam. In addition, it is better to have options other than the FEM. The method for deriving an exact solution using boundary conditions can be applied in the analysis of the vibration of beams without discretization. In this method, an expression that satisfies the equation of motion of the minute fraction was first obtained before the coefficients of the expression were determined using the boundary conditions (Bishop and Johnson, 1960; Yamada and Utsuno, 2020). Although an exact solution can be obtained using this method, there exist some problems. One is that a limited number of vibration systems can be analyzed using this method. For example, the exact solution for a beam cannot be obtained when the vibration is controlled using sensors and actuators. The second problem is that equations of motion for low degrees of freedom (DOFs) cannot be obtained. It is important to reduce the DOFs of vibration systems to capture the essence of physical phenomena. The third problem is that the simulation results numerically diverge in the high frequency region because the exact solution contains exponential functions. Modal analysis is a promising solution for these issues (Benaroya and Nagurka, 2009; Meirovitch, 1967, 1990, 2001; Nagamatsu, 1985; Rao, 2007; Reismann, 1988; Shabana, 1991). In this study, the eigenfunctions for the beams that are continuous and not discretized are considered. The vibration systems with sensors and actuators can be analyzed and the DOFs can be reduced using modal analysis (Yamada and Asami, 2022). When the boundary conditions at both ends of the beam are simple, such as clamped ends, free ends, supported ends, guided ends, displacement excitation, and angular displacement excitation, the vibration of the beam can be theoretically analyzed using conventional modal analysis (Yamada and Utsuno, 2020). When arbitrary impedances are installed at the beam boundaries, or when the boundaries are coupled with other structures, problems may be encountered in conventional modal analysis. In such cases, using a free-free beam for conventional modal analysis is the most natural choice and was thus employed. However, the following problems were encountered. The most significant problem was that even if the number of adopted eigenmodes was increased, simulation results could not be obtained with sufficient precision. Moreover, the precision of the simulation deteriorated as the impedances coupled to both ends increased. In addition, because the eigenfunctions of a free-free beam include exponential functions, the numerical values diverged in higher-order eigenmodes. The problem of exponential function divergence can be solved to some extent using an approximation. However, this measure is inconvenient in practice and produces errors. It is also practically inconvenient that the frequency equation can only be numerically solved using a free-free beam.

Therefore, an analytical method wherein the substructure elimination method and either a guided-guided or simply supported beam is used to solve these problems is proposed in this study (Yamada, 2017, 2018). In this study, the vibration of the beam is expressed using the superposition of the eigenmodes of the guided-guided beam or simply supported beam. Moreover, the eigenfunctions of both the guided-guided beam and simply supported beam do not include exponential functions, and the solutions of the frequency equations are expressed by algebraic expressions. In the substructure elimination method, the regions near both ends of the beam are eliminated and new boundaries are installed. The substructure elimination method for one-dimensional acoustic fields was reported in detail in a previous study (Yamada and Ji, 2023), where it was found that the variation in the phase of each eigenfunction at the new boundary coordinates yields sufficiently precise simulation results with fewer DOFs. This significant feature of the substructure elimination method for acoustic fields can be applied to beams. However, the substructure elimination method for beams has several problems because it was only briefly reported on by the first author (Yamada, 2017, 2018). First, a substructure elimination method using a simply supported beam was not proposed. Second, a versatile method for setting arbitrary boundary conditions on new boundaries was not developed. Third, the criteria for determining the line density, bending stiffness, and length of the elimination regions were not provided. Fourth, a criterion for determining the highest order of the eigenmode when the upper limit of the frequency range is given was not provided. To solve the first problem, a substructure elimination method for simply supported beams is described. To use a simply supported beam, a rigid body mode with a natural frequency of 0 Hz is required; thus, a deflection potential is introduced. Using a simply supported beam in addition to a guided-guided beam is considered as the second option. To solve the second problem, a new formulation method based on constraint conditions is presented. Modal analysis is applied to the equation of motion of the minute fraction, and equations of motion are derived using modal displacements. To solve the third and fourth problems, the appropriate material properties of the elimination regions and highest order of the eigenmode are determined through simulations. In this study, the effectiveness of the substructure elimination method is verified by comparing the simulation results obtained using the substructure elimination method based on the exact solutions obtained using boundary conditions. The simulation results obtained using the proposed method are also compared with those obtained using the conventional modal analysis with a free-free beam to investigate the advantage of the proposed

[DOI: 10.1299/mej.23-00293]
© 2023 The Japan Society of Mechanical Engineers

method for modal analysis using continuous functions.

2. Theoretical analysis

In this section, the equation of motion of the minute fraction of a Bernoulli-Euler beam when the regions near both ends are eliminated is derived first. The equations of motion of the minute fraction are derived using the deflection and deflection potential as variables. The equation of motion using deflection is used for the proposed method with a guided-guided beam, and the equation of motion using deflection potential is used for the proposed method with a simply supported beam. Second, the equations determined under the constraint conditions at the new boundaries are derived. Six types of boundaries are described: free end, clamped end, supported end, guided end, displacement and angular displacement excitation, and translational and rotational impedances using 1-DOF vibration systems. Third, modal analysis is applied to obtain equations of motion using modal displacements. The deflection, slope, bending moment, and shear force are also formulated.

2.1 Analytical model

The analytical models of the proposed methods using a guided-guided beam and simply supported beam are shown in Figs. 1(a) and (b), respectively. Here, the densities of the center region and left and right elimination regions are ρ_{A}, ρ_{B}, and ρ_{C}, respectively; their Young's moduli are E_{A}, E_{B}, and E_{C}, respectively; their widths are b_{A}, b_{B}, and b_{C}, respectively; their thicknesses are t_{A}, t_{B}, and t_{C}, respectively; their lengths are l_{A}, l_{B}, and l_{C}, respectively; the left ends of the beams are set to the origin of the x-coordinate; and the right-hand direction is the positive direction of the x-coordinate. The x-coordinates of the new left and right boundaries are $x_{\mathrm{B}}\left(=l_{\mathrm{B}}\right)$ and $x_{\mathrm{C}}\left(=l_{\mathrm{A}}+l_{\mathrm{B}}\right)$, respectively, and the overall length of the beams is $l_{\mathrm{ABC}}\left(=l_{\mathrm{A}}+l_{\mathrm{B}}+l_{\mathrm{C}}\right)$. Common symbols are used for the two types of beams. The center region and left and right elimination regions are referred to as regions A, B, and C, respectively. The cross-sectional areas of regions A, B, and C are $S_{\mathrm{A}}\left(=b_{\mathrm{A}}t_{\mathrm{A}}\right)$, $S_{\mathrm{B}}\left(=b_{\mathrm{B}}t_{\mathrm{B}}\right)$, and $S_{\mathrm{C}}\left(=b_{\mathrm{C}}t_{\mathrm{C}}\right)$, respectively, the second moments of area of regions A, B, and C are $I_{\mathrm{A}}\left(=b_{\mathrm{A}}t_{\mathrm{A}}^3/12\right)$, $I_{\mathrm{B}}\left(=b_{\mathrm{B}}t_{\mathrm{B}}^3/12\right)$, and $I_{\mathrm{C}}\left(=b_{\mathrm{C}}t_{\mathrm{C}}^3/12\right)$, respectively, the line densities of regions A, B, and C are $\mu_{\mathrm{A}}\left(=\rho_{\mathrm{A}}S_{\mathrm{A}}\right)$, $\mu_{\mathrm{B}}\left(=\rho_{\mathrm{B}}S_{\mathrm{B}}\right)$, and $\mu_{\mathrm{C}}\left(=\rho_{\mathrm{C}}S_{\mathrm{C}}\right)$, respectively, and the bending stiffnesses of regions A, B, and C are $D_{\mathrm{A}}\left(=E_{\mathrm{A}}I_{\mathrm{A}}\right)$, $D_{\mathrm{B}}\left(=E_{\mathrm{B}}I_{\mathrm{B}}\right)$, and $D_{\mathrm{C}}\left(=E_{\mathrm{C}}I_{\mathrm{C}}\right)$, respectively. In this study, only the cases with $\mu_{\mathrm{B}}=\mu_{\mathrm{C}}$ and $D_{\mathrm{B}}=D_{\mathrm{C}}$ were considered because regions B and C were eliminated in a similar manner. However, in the formulation, the symbols were separated to clearly distinguish between regions B and C. As shown in Figs. 1(a) and (b), the external forces f_{B} and f_{C} are applied to the new left and right boundaries in the downward direction, and bending moments N_{B} and N_{C} are applied to the new left and right boundaries in the clockwise direction. These external forces and bending moments are determined using the constraint conditions. In addition, the external force f_{ex} is applied as an excitation force in the downward direction at $x=x_f$, and the bending moment N_{ex} is applied as the excitation bending moment in the clockwise direction at $x=x_N$. When the beam is subjected to displacement and angular displacement excitation at the new boundaries, f_{ex} and N_{ex} would not be applied. In this case, $f_{\mathrm{ex}}=0$ and $N_{\mathrm{ex}}=0$ should be used. In this study, eliminating a region implies that the line density and bending stiffness of the region are set to zero or sufficiently small values such that the shear force and bending moment is zero or almost zero in that region. Although the shear force and bending moment are negligible in the elimination regions, the deflection and slope are not, and the deflection can adopt any value in the elimination regions. This is a mild condition for expressing

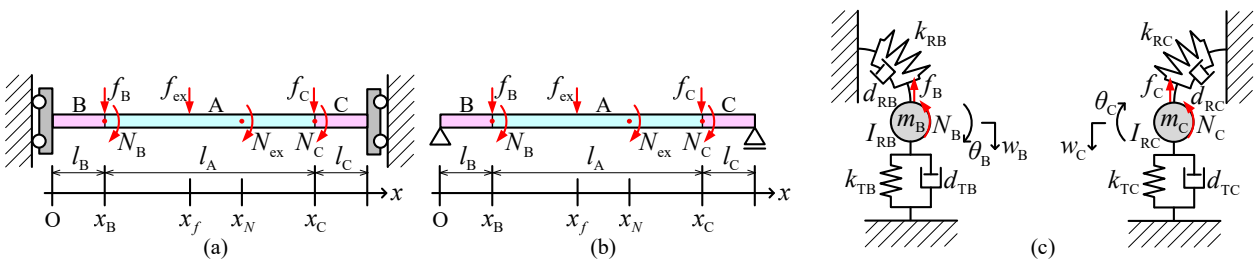

Fig. 1 Analytical models for the substructure elimination method using a guided-guided beam and simply supported beam, and 1-DOF vibration systems installed at the new boundaries: (a) analytical model using a guided-guided beam, (b) analytical model using a simply supported beam and (c) analytical models of the translational and rotational 1-DOF vibration systems installed at the new boundaries.

[DOI: 10.1299/mej.23-00293]
© 2023 The Japan Society of Mechanical Engineers

the vibration in region A using the superposition of the eigenmodes. The analytical models of the translational and rotational 1-DOF vibration systems installed at the new left and right boundaries are shown in Fig. 1(c). These 1-DOF vibration systems provide an arbitrary mechanical impedance at new boundaries. The mass, spring constant, viscous damping coefficient, and displacement of the translational 1-DOF vibration system installed at $x = x_{\mathrm{B}}$ are m_{B}, k_{TB}, d_{TB}, and w_{B}, respectively, those at $x = x_{\mathrm{C}}$ are m_{C}, k_{TC}, d_{TC}, and w_{C}, respectively, the moment of inertia, rotational spring constant, rotational viscous damping coefficient, and angular displacement of the rotational 1-DOF vibration system installed at $x = x_{\mathrm{B}}$ are I_{RB}, k_{RB}, d_{RB}, and θ_{B}, respectively, and those at $x = x_{\mathrm{C}}$ are I_{RC}, k_{RC}, d_{RC}, and θ_{C}, respectively. The positive direction of the displacements w_{B} and w_{C} is the downward direction, and that of the angular displacements θ_{B} and θ_{C} is the clockwise direction. Because of the action and reaction relationship, f_{B} and f_{C} are applied to the translational 1-DOF vibration systems in the upward direction, and N_{B} and N_{C} are applied to the rotational 1-DOF vibration systems in the counterclockwise direction.

2.2 Equations of motion of the minute fraction

When the guided-guided beam shown in Fig. 1(a) is used, the equation of motion of the minute fraction is expressed as

$$\begin{aligned}&\mu(x)\frac{\partial^2 w}{\partial t^2}+\frac{\partial^2}{\partial x^2}\left(D(x)\frac{\partial^2 w}{\partial x^2}\right)\\&=f_{\mathrm{B}}\delta(x-x_{\mathrm{B}})-N_{\mathrm{B}}\delta'(x-x_{\mathrm{B}})+f_{\mathrm{C}}\delta(x-x_{\mathrm{C}})-N_{\mathrm{C}}\delta'(x-x_{\mathrm{C}})+f_{\mathrm{ex}}\delta(x-x_f)-N_{\mathrm{ex}}\delta'(x-x_N)\end{aligned}, \tag{1}$$

$$\mu(x)=\mu_{\mathrm{A}}+\mu_{\mathrm{B\text{-}A}}H(x_{\mathrm{B}}-x)+\mu_{\mathrm{C\text{-}A}}H(x-x_{\mathrm{C}}),\quad D(x)=D_{\mathrm{A}}+D_{\mathrm{B\text{-}A}}H(x_{\mathrm{B}}-x)+D_{\mathrm{C\text{-}A}}H(x-x_{\mathrm{C}}), \tag{2}$$

$$\mu_{\mathrm{B\text{-}A}}=\mu_{\mathrm{B}}-\mu_{\mathrm{A}},\quad \mu_{\mathrm{C\text{-}A}}=\mu_{\mathrm{C}}-\mu_{\mathrm{A}},\quad D_{\mathrm{B\text{-}A}}=D_{\mathrm{B}}-D_{\mathrm{A}},\quad D_{\mathrm{C\text{-}A}}=D_{\mathrm{C}}-D_{\mathrm{A}}, \tag{3}$$

where w is the deflection of the beam, t is time, δ is the Dirac delta function, H is the Heaviside step function, and $'$ denotes $\partial/\partial x$ in this study. The positive direction of the deflection w is the downward direction. When the simply supported beam shown in Fig. 1(b) is used, the equation of motion is expressed as

$$\begin{aligned}&\mu(x)\frac{\partial^2\psi}{\partial t^2}-\mu_{\mathrm{B\text{-}A}}H(x_{\mathrm{B}}-x)\frac{\partial^2\psi}{\partial t^2}\bigg|_{x=x_{\mathrm{B}}}-\mu_{\mathrm{C\text{-}A}}H(x-x_{\mathrm{C}})\frac{\partial^2\psi}{\partial t^2}\bigg|_{x=x_{\mathrm{C}}}+\frac{\partial}{\partial x}\left(D(x)\frac{\partial^3\psi}{\partial x^3}\right)\\&=f_{\mathrm{B}}H(x_{\mathrm{B}}-x)+N_{\mathrm{B}}\delta(x-x_{\mathrm{B}})-f_{\mathrm{C}}H(x-x_{\mathrm{C}})+N_{\mathrm{C}}\delta(x-x_{\mathrm{C}})-f_{\mathrm{ex}}H(x-x_f)+N_{\mathrm{ex}}\delta(x-x_N)\end{aligned}, \tag{4}$$

where ψ is the deflection potential. The relationship between $w(x,t)$ and $\psi(x,t)$ is defined as

$$w(x,t)=-\frac{\partial\psi}{\partial x}. \tag{5}$$

The partial differentiation of both sides of Eq. (4) by x yields Eq. (1). For example, the first term on the right-hand side of Eq. (4) can be replaced by $-f_{\mathrm{B}}H(x-x_{\mathrm{B}})$ because the partial differentiations of $f_{\mathrm{B}}H(x_{\mathrm{B}}-x)$ and $-f_{\mathrm{B}}H(x-x_{\mathrm{B}})$ by x provide an identical expression. It is advantageous to use the terms given in Eq. (4) when deriving the shear force in region A because $f_{\mathrm{B}}H(x_{\mathrm{B}}-x)$ is zero in region A. The equation of motion expressed using the deflection potential ψ is essential when using the rigid body mode of a simply supported beam. This is essentially identical to using the displacement potential in a wave equation for a one-dimensional acoustic field (Yamada and Ji, 2023). The rigid body mode of a simply supported beam has no deflection and slope over the entire length of the beam, but has values of shear force and bending moment.

2.3 Equations derived using the constraint conditions

The case in which the new left and right boundaries have identical constraints is described in this section. These cases should be combined when the boundary conditions at both ends are different. If both cases, the one wherein the boundary is a free end and that comprising a combination of displacement and angular displacement excitation are understood, they can be used to consider the following three cases: clamped end, supported end, and guided end. Therefore, the two boundary conditions are first formulated before the other three types of boundary conditions are described. Lastly, the case in which translational and rotational impedances using 1-DOF vibration systems are installed is formulated.

[DOI: 10.1299/mej.23-00293]
© 2023 The Japan Society of Mechanical Engineers

If the new left and right boundaries are free ends, the shear forces and bending moments at the new boundaries are zero. Therefore, the equations determined using the boundary conditions are given as

$$f_{\mathrm{B}} = f_{\mathrm{C}} = 0, \quad N_{\mathrm{B}} = N_{\mathrm{C}} = 0. \tag{6}$$

In this case, the four unknown variables f_{B}, f_{C}, N_{B}, and N_{C} in Eqs. (1) and (4) are directly determined.

If the new left and right boundary conditions are obtained using a combination of displacement and angular displacement excitation, the equations determined using the constraint conditions are expressed as

$$w(x_{\mathrm{B}}, t) = w_{\mathrm{L}}(t), \quad \left.\frac{\partial w}{\partial x}\right|_{x=x_{\mathrm{B}}} = \theta_{\mathrm{L}}(t), \quad w(x_{\mathrm{C}}, t) = w_{\mathrm{R}}(t), \quad \left.\frac{\partial w}{\partial x}\right|_{x=x_{\mathrm{C}}} = \theta_{\mathrm{R}}(t), \tag{7}$$

where w_{L} and w_{R} are the displacements applied at the new left and right boundaries, and θ_{L} and θ_{R} are the angular displacements. The four unknown variables f_{B}, f_{C}, N_{B}, and N_{C} in Eqs. (1) and (4) cannot be determined using Eq. (7). To formulate these four unknown variables, modal analysis must be applied. Therefore, the details on the formulation are described in Section 2.4.

If the new left and right boundaries are clamped ends, $w_{\mathrm{L}} = w_{\mathrm{R}} = 0$ and $\theta_{\mathrm{L}} = \theta_{\mathrm{R}} = 0$ should be used in Eq. (7). The clamped end can be regarded as a special case comprising the combination of displacement and angular displacement excitation.

If the new left and right boundaries are simply supported ends, $w_{\mathrm{L}} = w_{\mathrm{R}} = 0$ in Eq. (7) and $N_{\mathrm{B}} = N_{\mathrm{C}} = 0$ should be used. In contrast, if the new left and right boundaries are guided ends, $f_{\mathrm{B}} = f_{\mathrm{C}} = 0$ and $\theta_{\mathrm{L}} = \theta_{\mathrm{R}} = 0$ in Eq. (7) should be used.

When the translational and rotational impedances using 1-DOF vibration systems are installed at the new left and right boundaries, the equations of motion for the 1-DOF vibration systems are derived as

$$m_{\mathrm{B}}\ddot{w}_{\mathrm{B}} + d_{\mathrm{TB}}\dot{w}_{\mathrm{B}} + k_{\mathrm{TB}}w_{\mathrm{B}} = -f_{\mathrm{B}}, \quad I_{\mathrm{RB}}\ddot{\theta}_{\mathrm{B}} + d_{\mathrm{RB}}\dot{\theta}_{\mathrm{B}} + k_{\mathrm{RB}}\theta_{\mathrm{B}} = -N_{\mathrm{B}}, \tag{8}$$

$$m_{\mathrm{C}}\ddot{w}_{\mathrm{C}} + d_{\mathrm{TC}}\dot{w}_{\mathrm{C}} + k_{\mathrm{TC}}w_{\mathrm{C}} = -f_{\mathrm{C}}, \quad I_{\mathrm{RC}}\ddot{\theta}_{\mathrm{C}} + d_{\mathrm{RC}}\dot{\theta}_{\mathrm{C}} + k_{\mathrm{RC}}\theta_{\mathrm{C}} = -N_{\mathrm{C}}. \tag{9}$$

The four unknown variables f_{B}, f_{C}, N_{B}, and N_{C} are determined using these equations. However, w_{B}, θ_{B}, w_{C}, and θ_{C} are the new unknown variables in this case. Because w_{B}, θ_{B}, w_{C}, and θ_{C} must be equal to the displacements and slopes of the beam at the new boundaries, these four variable can be determined using:

$$w_{\mathrm{B}}(t) = w(x_{\mathrm{B}}, t), \quad \theta_{\mathrm{B}}(t) = \left.\frac{\partial w}{\partial x}\right|_{x=x_{\mathrm{B}}}, \quad w_{\mathrm{C}}(t) = w(x_{\mathrm{C}}, t), \quad \theta_{\mathrm{C}}(t) = \left.\frac{\partial w}{\partial x}\right|_{x=x_{\mathrm{C}}}. \tag{10}$$

2.4 Modal analysis

In this section, the equations of motion with modal displacements for the guided-guided beam and simply supported beam are first derived. Subsequently, the equations derived using the constraint conditions are then expressed using the modal displacements. The equations of motion with no unknown variables other than the modal displacements are then formulated. Lastly, the slope, bending moment, and shear force are formulated to express them with the modal displacements.

In the substructure elimination method, the deflection w or deflection potential ψ is expressed using the superposition of the eigenmodes before eliminating regions B and C. This refers to the eigenmodes when the line densities and bending stiffnesses of regions B and C are μ_{A} and D_{A}, respectively. When a guided-guided beam is used, the deflection w is expressed as

$$w(x, t) = \sum_{h=0}^{n} W_h(x)\xi_h(t), \quad W_h(x) = A_h \cos k_h x, \quad k_h = \frac{h\pi}{l_{\mathrm{ABC}}}, \tag{11}$$

where W_h is the eigenfunction of the deflection, ξ_h is the modal displacement, the subscript h denotes the hth-order of the eigenmode, n is the highest order of the eigenmode, A_h is the arbitrary constant, and k_h is the wave number. In this case, the deflection is obtained using a Fourier cosine series. The following equations of motion are obtained using modal displacements by substituting Eq. (11) into the Eq. (1), multiplying both the sides by W_i/μ_{A}, and integrating over the entire range of the beam:

[DOI: 10.1299/mej.23-00293]
© 2023 The Japan Society of Mechanical Engineers

$$M_i\ddot{\xi}_i+\frac{\mu_{\text{B-A}}}{\mu_{\text{A}}}\sum_{h=0}^{n}\int_0^{x_{\text{B}}}W_hW_i\mathrm{d}x\ddot{\xi}_h+\frac{\mu_{\text{C-A}}}{\mu_{\text{A}}}\sum_{h=0}^{n}\int_{x_{\text{C}}}^{l_{\text{ABC}}}W_hW_i\mathrm{d}x\ddot{\xi}_h+K_i\xi_i$$
$$+\frac{D_{\text{B-A}}}{\mu_{\text{A}}}\sum_{h=1}^{n}\left[k_h^4\int_0^{x_{\text{B}}}W_hW_i\mathrm{d}x+\left(W_h''W_i'-W_h'''W_i\right)\Big|_{x=x_{\text{B}}}\right]\xi_h+\frac{D_{\text{C-A}}}{\mu_{\text{A}}}\sum_{h=1}^{n}\left[k_h^4\int_{x_{\text{C}}}^{l_{\text{ABC}}}W_hW_i\mathrm{d}x-\left(W_h''W_i'-W_h'''W_i\right)\Big|_{x=x_{\text{C}}}\right]\xi_h\,, \tag{12}$$
$$=\frac{W_i\left(x_{\text{B}}\right)}{\mu_{\text{A}}}f_{\text{B}}+\frac{W_i'\left(x_{\text{B}}\right)}{\mu_{\text{A}}}N_{\text{B}}+\frac{W_i\left(x_{\text{C}}\right)}{\mu_{\text{A}}}f_{\text{C}}+\frac{W_i'\left(x_{\text{C}}\right)}{\mu_{\text{A}}}N_{\text{C}}+\frac{W_i\left(x_f\right)}{\mu_{\text{A}}}f_{\text{ex}}+\frac{W_i'\left(x_N\right)}{\mu_{\text{A}}}N_{\text{ex}}$$

$$M_i=\int_0^{l_{\text{ABC}}}W_i^2\mathrm{d}x=1\,,\quad K_i=\omega_i^2\,,\quad \omega_i=k_i^2\sqrt{\frac{D_{\text{A}}}{\mu_{\text{A}}}}\,,\quad A_i=\begin{cases}\sqrt{\dfrac{1}{l_{\text{ABC}}}} & (i=0)\\ \sqrt{\dfrac{2}{l_{\text{ABC}}}} & (i=1,\,2,\,\cdots)\end{cases}, \tag{13}$$

where M_i and K_i are the modal mass and modal stiffness, respectively, of the original beam without elimination, and ω_i is the natural angular frequency of the *i*th-order eigenmode of the original beam. The arbitrary constant A_i of the eigenfunction was normalized so that $M_i=1$ in this study. The second and fifth terms on the left-hand side of Eq. (12) are the results of the elimination of region B, and the third and sixth terms are the results of the elimination of region C.

When a simply supported beam is used, the deflection potential ψ is used, and it is expressed as

$$\psi\left(x,\,t\right)=\sum_{h=0}^{n}\Psi_h\left(x\right)\xi_h\left(t\right)\,,\quad \Psi_h\left(x\right)=A_h\cos k_hx\,, \tag{14}$$

where the same symbols as those used for the guided-guided beam are used for the modal displacement, arbitrary constant, and wave number. The wave number k_h is also obtained using Eq. (11). In this case, the deflection potential is obtained using a Fourier cosine series, and the deflection is expressed using a Fourier sine series. The following equations of motion are obtained using modal displacements by substituting Eq. (14) into the Eq. (4), multiplying both the sides by Ψ_i/μ_{A}, and integrating over the entire range of the beam:

$$M_i\ddot{\xi}_i+\frac{\mu_{\text{B-A}}}{\mu_{\text{A}}}\sum_{h=0}^{n}\left(\int_0^{x_{\text{B}}}\Psi_h\Psi_i\mathrm{d}x-\Psi_h\left(x_{\text{B}}\right)\int_0^{x_{\text{B}}}\Psi_i\mathrm{d}x\right)\ddot{\xi}_h+\frac{\mu_{\text{C-A}}}{\mu_{\text{A}}}\sum_{h=0}^{n}\left(\int_{x_{\text{C}}}^{l_{\text{ABC}}}\Psi_h\Psi_i\mathrm{d}x-\Psi_h\left(x_{\text{C}}\right)\int_{x_{\text{C}}}^{l_{\text{ABC}}}\Psi_i\mathrm{d}x\right)\ddot{\xi}_h+K_i\xi_i$$
$$+\frac{D_{\text{B-A}}}{\mu_{\text{A}}}\sum_{h=1}^{n}\left[k_h^4\int_0^{x_{\text{B}}}\Psi_h\Psi_i\mathrm{d}x-\left(\Psi_h'''\Psi_i\right)\Big|_{x=x_{\text{B}}}\right]\xi_h+\frac{D_{\text{C-A}}}{\mu_{\text{A}}}\sum_{h=1}^{n}\left[k_h^4\int_{x_{\text{C}}}^{l_{\text{ABC}}}\Psi_h\Psi_i\mathrm{d}x+\left(\Psi_h'''\Psi_i\right)\Big|_{x=x_{\text{C}}}\right]\xi_h \tag{15}$$
$$=\frac{\int_0^{x_{\text{B}}}\Psi_i\mathrm{d}x}{\mu_{\text{A}}}f_{\text{B}}+\frac{\Psi_i\left(x_{\text{B}}\right)}{\mu_{\text{A}}}N_{\text{B}}-\frac{\int_{x_{\text{C}}}^{l_{\text{ABC}}}\Psi_i\mathrm{d}x}{\mu_{\text{A}}}f_{\text{C}}+\frac{\Psi_i\left(x_{\text{C}}\right)}{\mu_{\text{A}}}N_{\text{C}}-\frac{\int_{x_f}^{l_{\text{ABC}}}\Psi_i\mathrm{d}x}{\mu_{\text{A}}}f_{\text{ex}}+\frac{\Psi_i\left(x_N\right)}{\mu_{\text{A}}}N_{\text{ex}}$$

$$M_i=\int_0^{l_{\text{ABC}}}\Psi_i^2\mathrm{d}x=1\,. \tag{16}$$

The modal stiffness K_i, the natural angular frequency ω_i, and arbitrary constant A_i are obtained using Eq. (13), respectively. The arbitrary constant A_i was normalized so that $M_i=1$. The second and fifth terms on the left-hand side of Eq. (15) are the results of the elimination of region B, and the third and sixth terms are the results of the elimination of region C.

In both cases using a guided-guided beam and simply supported beam, the equation of motion using matrices are expressed as

$$[M]\left\{\ddot{\xi}\right\}+[K]\{\xi\}=[H]\left\{f_{\text{BC}}\right\}+[Q]\{f\}\,, \tag{17}$$

$$\{\xi\}=\left\{\xi_0\quad\xi_1\quad\cdots\quad\xi_n\right\}^{\text{T}}\,,\quad\left\{f_{\text{BC}}\right\}=\left\{f_{\text{B}}\quad N_{\text{B}}\quad f_{\text{C}}\quad N_{\text{C}}\right\}^{\text{T}}\,,\quad\{f\}=\left\{f_{\text{ex}}\quad N_{\text{ex}}\right\}^{\text{T}}\,, \tag{18}$$

where $[M]$ is the mass matrix, which is a square matrix of size $n+1$; $[K]$ is the stiffness matrix, which is a square matrix of size $n+1$; $[H]$ is the external force and bending moment influence matrix determined by the constraint conditions, which is an $(n+1)$-by-4 matrix; and $[Q]$ is the excitation force and bending moment influence matrix, which is an $(n+1)$-by-2 matrix. Moreover, $\{\xi\}$ is the modal displacement vector, $\left\{f_{\text{BC}}\right\}$ is the external force and bending moment vector, $\{f\}$ is the excitation force and bending moment vector, and the superscript T denotes the transpose of the matrix. Each element of matrices $[M]$, $[K]$, $[H]$, and $[Q]$ can be obtained using Eq. (12) or (15)

[DOI: 10.1299/mej.23-00293]
© 2023 The Japan Society of Mechanical Engineers

for each case using a guided-guided beam or simply supported beam.

When the new left and right boundaries are free ends, $\{f_{\mathrm{BC}}\}=\{0 \quad 0 \quad 0 \quad 0\}^{\mathrm{T}}$. Therefore, the first term on the right-hand side of Eq. (17) disappears in this case. When both the new boundaries are set to the combination of the displacement and angular displacement excitation, from Eqs. (7) and (11), the equations obtained using the constraint conditions for the guided-guided beam case are expressed as

$$\sum_{h=0}^{n} W_h(x_{\mathrm{B}})\xi_h(t)=w_{\mathrm{L}},\ \sum_{h=0}^{n} W_h'(x_{\mathrm{B}})\xi_h(t)=\theta_{\mathrm{L}},\ \sum_{h=0}^{n} W_h(x_{\mathrm{C}})\xi_h(t)=w_{\mathrm{R}},\ \sum_{h=0}^{n} W_h'(x_{\mathrm{C}})\xi_h(t)=\theta_{\mathrm{R}}. \tag{19}$$

From Eqs. (5), (7), and (14), the equations for the simply supported beam case are derived as

$$-\sum_{h=1}^{n} \Psi_h'(x_{\mathrm{B}})\xi_h(t)=w_{\mathrm{L}},\ -\sum_{h=1}^{n} \Psi_h''(x_{\mathrm{B}})\xi_h(t)=\theta_{\mathrm{L}},\ -\sum_{h=1}^{n} \Psi_h'(x_{\mathrm{C}})\xi_h(t)=w_{\mathrm{R}},\ -\sum_{h=1}^{n} \Psi_h''(x_{\mathrm{C}})\xi_h(t)=\theta_{\mathrm{R}}. \tag{20}$$

In both cases, Eq. (19) and Eq. (20), which were derived using the constraint conditions, can be written as

$$[C]\{\xi\}=\{w_{\mathrm{LR}}\},\ \{w_{\mathrm{LR}}\}=\{w_{\mathrm{L}} \quad \theta_{\mathrm{L}} \quad w_{\mathrm{R}} \quad \theta_{\mathrm{R}}\}^{\mathrm{T}}, \tag{21}$$

where $[C]$ is the constraint condition matrix, which is a 4-by-$(n+1)$ matrix, and $\{w_{\mathrm{LR}}\}$ is the displacement excitation vector. Each element of matrix $[C]$ can be obtained using Eq. (19) or Eq. (20). However, Eq. (21) cannot be used to directly determine $\{f_{\mathrm{BC}}\}$; thus, Eqs. (17) and (21) are used. Moreover, innumerable methods are available. Therefore, only the most useful method was investigated and described herein. However, there is no guarantee that the method considered, which reduces the number of inverse matrix calculations to suppress the deterioration of the precision, is the optimum method. First, Eq. (17) is transformed as follows:

$$([I]+[M_{\mathrm{R}}])\{\ddot{\xi}\}+[K]\{\xi\}=[H]\{f_{\mathrm{BC}}\}+[Q]\{f\},\ [M_{\mathrm{R}}]=[M]-[I], \tag{22}$$

where $[I]$ is the identity matrix, which is a square matrix of size $n+1$. $[I]$ can be regarded as a matrix consisting only of the first terms on the left-hand side of Eq. (12) or (15). Additionally, the following equation can be derived from Eq. (22):

$$\{\ddot{\xi}\}=-[M_{\mathrm{R}}]\{\ddot{\xi}\}-[K]\{\xi\}+[H]\{f_{\mathrm{BC}}\}+[Q]\{f\}. \tag{23}$$

The following equation is obtained by performing second-order differentiation on both sides of Eq. (21) with respect to the time and substituting Eq. (23):

$$-[C][M_{\mathrm{R}}]\{\ddot{\xi}\}-[C][K]\{\xi\}+[C][H]\{f_{\mathrm{BC}}\}+[C][Q]\{f\}=\{\ddot{w}_{\mathrm{LR}}\}, \tag{24}$$

where the constraint conditions were used as acceleration constraints rather than displacement constraints. Subsequently, $\{f_{\mathrm{BC}}\}$ is obtained as follows:

$$\{f_{\mathrm{BC}}\}=([C][H])^{-1}\left([C][M_{\mathrm{R}}]\{\ddot{\xi}\}+[C][K]\{\xi\}-[C][Q]\{f\}+\{\ddot{w}_{\mathrm{LR}}\}\right). \tag{25}$$

From Eqs. (17) and (25), the equation of motion without using $\{f_{\mathrm{BC}}\}$ is expressed as

$$([M]-[D_{HC}][M_{\mathrm{R}}])\{\ddot{\xi}\}+([I]-[D_{HC}])[K]\{\xi\}=([I]-[D_{HC}])[Q]\{f\}+[H]([C][H])^{-1}\{\ddot{w}_{\mathrm{LR}}\}, \tag{26}$$

$$[D_{HC}]=[H]([C][H])^{-1}[C]. \tag{27}$$

The mass matrix was separated using the identity matrix in Eq. (22). If the stiffness matrix is separated using the identity matrix rather than the mass matrix, the constraint conditions can be used as displacement constraints. However, the precision of the simulations wherein displacement constraints were used is significantly lower than that wherein acceleration constrains were used.

If the translational and rotational impedances using 1-DOF vibration systems are installed at the new left and right boundaries, Eqs. (8)–(10), and (11), or Eqs. (5), (8)–(10), and (14), can be used to express $\{f_{\mathrm{BC}}\}$ as

[DOI: 10.1299/mej.23-00293]
© 2023 The Japan Society of Mechanical Engineers

$$\{f_{\mathrm{BC}}\} = -[M_m]\{\ddot{\xi}\} - [D_d]\{\dot{\xi}\} - [K_k]\{\xi\}, \tag{28}$$

where $[M_m]$, $[D_d]$, and $[K_k]$ are 4-by-$(n+1)$ matrices. Each element of matrices $[M_m]$, $[D_d]$, and $[K_k]$ can be obtained using Eqs. (8)–(10), and (11), or Eqs. (5), (8)–(10), and (14). The equation of motion without using $\{f_{\mathrm{BC}}\}$ can be obtained as follows by substituting Eq. (28) into Eq. (17):

$$\left([M]+[H][M_m]\right)\{\ddot{\xi}\} + [H][D_d]\{\dot{\xi}\} + \left([K]+[H][K_k]\right)\{\xi\} = [Q]\{f\}. \tag{29}$$

When $[H][D_d]$ is a Rayleigh damping matrix, an eigenvalue analysis can be performed using Eq. (29). When $[H][D_d]$ is not a Rayleigh damping matrix, eigenvalue analysis should be performed after deriving the equation of state using Eq. (29) for state-space representation. The uncoupled equations can be obtained using eigenvectors.

The slope, bending moment, and shear force are defined as

$$\theta(x,t) = \frac{\partial w}{\partial x} = -\frac{\partial^2 \psi}{\partial x^2}, \quad N(x,t) = -D(x)\frac{\partial^2 w}{\partial x^2} = D(x)\frac{\partial^3 \psi}{\partial x^3}, \tag{30}$$

$$f_{\mathrm{S}}(x,t) = -\frac{\partial}{\partial x}\left(D(x)\frac{\partial^2 w}{\partial x^2}\right) = \frac{\partial}{\partial x}\left(D(x)\frac{\partial^3 \psi}{\partial x^3}\right), \tag{31}$$

respectively. The deflection $w(x,t)$ and deflection potential $\psi(x,t)$ are obtained using Eqs. (11) and (14), respectively. For example, when evaluating the bending moment and shear force at $x = x_{\mathrm{B}}$, the values in region A should be obtained. Therefore, the value of the Heaviside step function in this case should be obtained using $x = x_{\mathrm{B}} + 0$. This should also be used in later equations for terms involving Dirac delta functions. When the beam is excited with f_{ex} or N_{ex} at a point other than the ends, the beam has a discontinuity in the shear force or bending moment diagram at the point. Therefore, the Gibbs phenomena occurs when the bending moment and shear force are obtained using Eqs. (30) and (31). This problem can be solved using the equation of motion of the minute fraction. When a guided-guided beam is used, integrating both sides of Eq. (1) from 0 to x once and twice, respectively, yields the following equations for the shear force and bending moment:

$$\begin{aligned} f_{\mathrm{S}}(x,t) = -\frac{\partial}{\partial x}\left(D(x)\frac{\partial^2 w}{\partial x^2}\right) = {} & \int_0^x \mu(x)\frac{\partial^2 w}{\partial t^2}\mathrm{d}x - f_{\mathrm{B}}H(x-x_{\mathrm{B}}) + N_{\mathrm{B}}\delta(x-x_{\mathrm{B}}) \\ & - f_{\mathrm{C}}H(x-x_{\mathrm{C}}) + N_{\mathrm{C}}\delta(x-x_{\mathrm{C}}) - f_{\mathrm{ex}}H(x-x_f) + N_{\mathrm{ex}}\delta(x-x_N) \end{aligned}, \tag{32}$$

$$\begin{aligned} N(x,t) = -D(x)\frac{\partial^2 w}{\partial x^2} = {} & \left(-D(x)\frac{\partial^2 w}{\partial x^2}\right)\Bigg|_{x=0} + \int_0^x\int_0^x \mu(x)\frac{\partial^2 w}{\partial t^2}\mathrm{d}x\mathrm{d}x - f_{\mathrm{B}}R(x-x_{\mathrm{B}}) + N_{\mathrm{B}}H(x-x_{\mathrm{B}}) \\ & - f_{\mathrm{C}}R(x-x_{\mathrm{C}}) + N_{\mathrm{C}}H(x-x_{\mathrm{C}}) - f_{\mathrm{ex}}R(x-x_f) + N_{\mathrm{ex}}H(x-x_N) \end{aligned}, \tag{33}$$

where R is the ramp function. When the shear force and bending moment in region A are considered, some terms in Eqs. (32) and (33) can be omitted. In addition, the Dirac delta function term $N_{\mathrm{ex}}\delta(x-x_N)$ can be omitted in Eq. (32). This is because the Dirac delta function only has a physical meaning after integration. For example, when a simply supported beam is subjected to a static bending moment at the center, the bending moment diagram has a discontinuity at the center. If the bending moment is differentiated by x to obtain the shear force, the shear force at the center becomes infinite. However, the actual shear force at the center is not infinite because the loads are only applied at both ends. Moreover, it is not necessary to consider the Dirac delta function when determining the shear force although it is generated by differentiating a discontinuity. Using Eqs. (32) and (33), discontinuities can be expressed using the Heaviside step function, and the non-smooth points are represented using a ramp function.

If a simply supported beam is used, the shear force is derived as

$$\begin{aligned} f_{\mathrm{S}}(x,t) = \frac{\partial}{\partial x}\left(D(x)\frac{\partial^3 \psi}{\partial x^3}\right) = {} & -\mu(x)\frac{\partial^2 \psi}{\partial t^2} + \left(\mu_{\text{B-A}}\frac{\partial^2 \psi}{\partial t^2}\Bigg|_{x=x_{\mathrm{B}}} + f_{\mathrm{B}}\right)H(x_{\mathrm{B}}-x) + N_{\mathrm{B}}\delta(x-x_{\mathrm{B}}) \\ & + \left(\mu_{\text{C-A}}\frac{\partial^2 \psi}{\partial t^2}\Bigg|_{x=x_{\mathrm{C}}} - f_{\mathrm{C}}\right)H(x-x_{\mathrm{C}}) + N_{\mathrm{C}}\delta(x-x_{\mathrm{C}}) - f_{\mathrm{ex}}H(x-x_f) + N_{\mathrm{ex}}\delta(x-x_N) \end{aligned}. \tag{34}$$

[DOI: 10.1299/mej.23-00293]
© 2023 The Japan Society of Mechanical Engineers

This equation can be obtained using Eq. (4). Additionally, the following equation for the bending moment can be obtained by integrating both sides of Eq. (4) from 0 to x:

$$N(x,t)=D(x)\frac{\partial^3\psi}{\partial x^3}=-\int_0^x\mu(x)\frac{\partial^2\psi}{\partial t^2}\mathrm{d}x+\left(\mu_{\text{B-A}}\left.\frac{\partial^2\psi}{\partial t^2}\right|_{x=x_{\text{B}}}+f_{\text{B}}\right)\left(x-R(x-x_{\text{B}})\right)+N_{\text{B}}H(x-x_{\text{B}})$$
$$+\left(\mu_{\text{C-A}}\left.\frac{\partial^2\psi}{\partial t^2}\right|_{x=x_{\text{C}}}-f_{\text{C}}\right)R(x-x_{\text{C}})+N_{\text{C}}H(x-x_{\text{C}})-f_{\text{ex}}R(x-x_f)+N_{\text{ex}}H(x-x_N) \quad (35)$$

When the shear force and bending moment in region A are considered, some terms in Eqs. (34) and (35) can be omitted. In addition, the Dirac delta function term $N_{\text{ex}}\delta(x-x_N)$ in Eq. (34) can be omitted for the same reason as that when a guided-guided beam is used. Because the series with a lower order of differentiation is more advantageous, Eqs. (32)–(35) were used for obtaining the shear force and bending moment in the simulations of this study.

3. Verifications through simulation

In this section, the criteria for determining the line density, bending stiffness, and length of the elimination regions are established through simulations. Preferably, the line density and bending stiffness in the elimination regions are zero because the translational and rotational mechanical impedance of the elimination region is zero. Therefore, the cases in which only the length of the elimination regions was varied and the line density and bending stiffness were zero were first considered. Subsequently, the cases in which the line density and bending stiffness had small values were considered. Furthermore, the precision of the natural frequencies obtained by eigenvalue analysis was investigated to determine the highest order n of the eigenmode of the original beam. In these simulations, the new boundaries were either guided or supported because the exact natural frequencies and eigenfunctions are expressed using simple algebraic equations. To verify the cases in which the new boundary is obtained for displacement and angular displacement excitation, clamped end, and free end, the simulation results for a beam subjected to displacement and angular displacement excitation at the new left boundary and clamped at the new right boundary, and a beam which is free at the new left boundary and subjected to a displacement and angular displacement excitation at the new right boundary, are presented. To verify that the substructure elimination method is more precise than the conventional modal analysis using a free-free beam, the simulation results for the conventional method and substructure elimination method are also presented in this section. In these simulations, a translational and rotational 1-DOF vibration systems were installed at the new boundaries, and the beam was excited using an external force and bending moment at the center of the beam. Because the proposed method was compared in several cases with the exact solution and conventional modal analysis using a free-free beam, the derivations for these methods are briefly described.

3.1 Verification of the length of the elimination region

Both the guide-guided beam and simply supported beam were used as the original beam in the simulations performed to verify the lengths of the elimination regions. In addition, the guided ends and supported ends were used as the new boundaries because the exact natural frequencies could be obtained. The material properties used in the simulations are listed in Table 1. Regardless of whether both the new boundaries were guided or supported, the exact natural frequencies were obtained using the square of the natural numbers and based on these material properties, excluding the rigid body mode. The elimination lengths l_{B} and l_{C} were maintained equal in these simulations. The relationship between the lengths of the elimination regions and precision of the natural frequencies was also evaluated through simulations, where the natural frequency of the highest order eigenmode of the original beam varied with n and l_{ABC}. $n=20$, 30, and 50 were used in these simulations. The root mean square (RMS) of the error rates of the natural frequencies was evaluated as the precision of the natural frequencies. The 1st–8th-order eigenmodes for $n=20$, 1st–16th-order eigenmodes for $n=30$, and 1st–32nd-order eigenmodes for $n=50$ were used to calculate the RMS of the error rates of the natural

Table 1 Material properties used in the simulations for the verification of the length of the elimination regions.

μ_{A}	0.2 kg/m	$\mu_{\text{B}}=\mu_{\text{C}}$	0 kg/m
D_{A}	0.8 Nm^2	$D_{\text{B}}=D_{\text{C}}$	0 Nm^2
$D_{\text{A}}/\mu_{\text{A}}$	4 m^4/s^2	l_{A}	$\sqrt{\pi}\approx1.772$ m

[DOI: 10.1299/mej.23-00293]
© 2023 The Japan Society of Mechanical Engineers

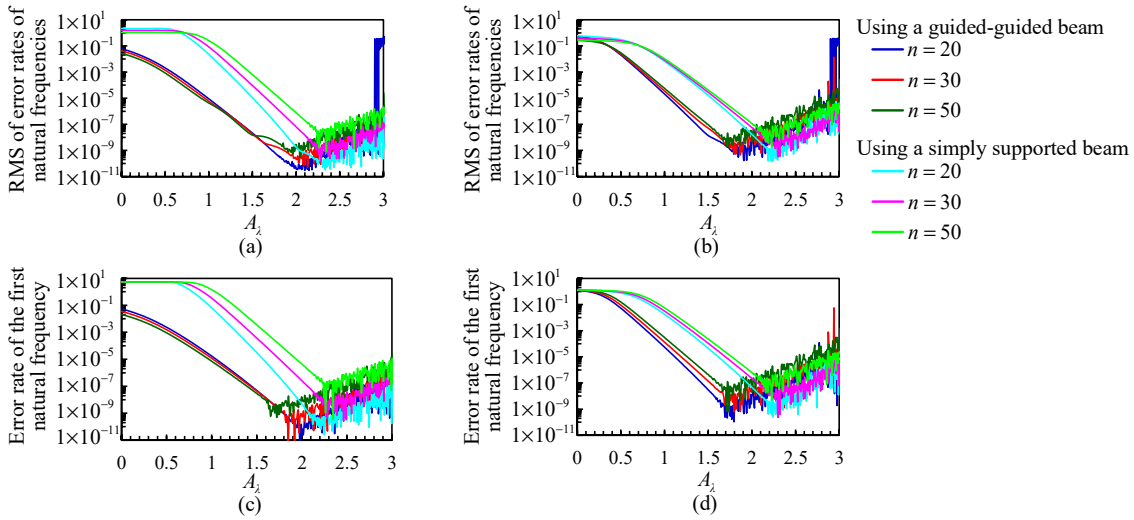

Fig. 2 Simulation results for the error rates of the natural frequencies obtained via the substructure elimination method using a guided-guided beam and simply supported beam: (a) RMS of the error rates of the multiple natural frequencies of guided ends on the new boundaries, (b) RMS of the error rates of the multiple natural frequencies of supported ends on the new boundaries, (c) magnitude of the error rate of the first natural frequency of guided ends on the new boundaries, and (d) magnitude of the error rate of the first natural frequency of supported ends on the new boundaries.

frequencies. The simulation results for the two types of original beams setting guided ends and supported ends on the new boundaries are shown in Figs. 2(a) and (b), respectively, and the simulation results for the error rate of the first-order natural frequency are shown in Figs. 2(c) and (d). The number of wavelengths A_λ on the horizontal axes is defined as follows:

$$A_\lambda = \frac{l_\mathrm{B}}{\lambda_n} = \frac{l_\mathrm{C}}{\lambda_n}, \quad \lambda_n = \frac{2l_\mathrm{ABC}}{n}, \tag{36}$$

where λ_n is the wavelength of the highest nth-order eigenmode of the original beam. As the number of wavelengths A_λ increases, the precision of the natural frequencies should improve because of the variation in the phases of the eigenfunctions at the new boundaries. However, the precision deteriorated from approximately $A_\lambda = 2$ in all cases. This was because the condition number of the matrix also deteriorated. The decrease in precision owing to the matrix condition number depends on the software and functions used in the eigenvalue analysis. The eigs function of MATLAB was used for simulations in this study. In addition, the inverse of the mass matrix was multiplied by the left side of the stiffness matrix to perform the eigenvalue analysis as a standard eigenvalue problem. The effect of the condition number of the matrix also changes when the eigenvalue analysis is performed as a generalized eigenvalue problem rather than a standard eigenvalue problem. Comparing the two types of original beams, the guided-guided beam is superior to the simply supported beam in terms of precision. However, considering practical use, a simply supported beam also provides sufficient precision. The error rate was high around $A_\lambda = 0$ when a simply supported beam was used to set the guided ends at the new boundaries. This was because deflection was constrained at both ends of the simply supported beam. A portion of the elimination length is required to set the guided ends at the new boundaries because guided ends have deflection. Depending on the strength of the constraint, the deflection restraint has a larger effect than the slope restraint, and simply supported beams require longer elimination regions than guided-guided beams. When guided ends are set at the new boundaries using a guided-guided beam and when supported ends are set at the new boundaries using a simply supported beam, the authors initially thought that the error rates should be small around $A_\lambda = 0$. However, this is not the case in Fig. 2. This is because, for example, when guided ends are set at the new boundaries using a guided-guided beam and $A_\lambda \approx 0$, the slopes and bending moments are zero at the new boundaries. However, the shear forces are not zero at the new boundaries. When supported ends are set at the new boundaries using a simply supported beam and $A_\lambda \approx 0$, the deflections and slopes are zero at the new boundaries. However, the bending moments are not zero at the new boundaries. In the latter case, the new boundaries are clamped rather than supported. Therefore, the error rates are not small around $A_\lambda = 0$ in Fig. 2. Moreover, the trend in the error rate of the first eigenmode is similar to that of multiple eigenmodes. Therefore, the precision can only be evaluated using the error rate of the first eigenmode. The validity of this fact can be

[DOI: 10.1299/mej.23-00293]
© 2023 The Japan Society of Mechanical Engineers

confirmed from the simulation results presented in Section 3.3. From the simulation results presented in Fig. 2, the A_λ at which the error rate of the natural frequencies is minimized does not depend on n. In these simulations, the lengths of the elimination regions were varied while maintaining $l_\mathrm{B} = l_\mathrm{C}$. Although the simulation results were omitted, a similar tendency was observed when one length was fixed and the other was varied. In our simulation environment, A_λ should be selected such that $1.5 \le A_\lambda \le 2.5$. Choosing a small value of A_λ that is within an acceptable range of precision loss is an option because a large value of A_λ requires a large ratio of the elimination regions, particularly for small values of n.

The 1st–8th-order eigenmodes for $n = 20$, 1st–16th-order eigenmodes for $n = 30$, and 1st–32nd-order eigenmodes for $n = 50$ were used in these simulations. Under the condition of $A_\lambda = 2.5$, the natural frequencies of the highest nth-order eigenmode of the original beam are 100, 400, and 1600 Hz, respectively. Because these are equal to the natural frequencies of the 10th, 20th, and 40th eigenmodes of a guided-guided beam and simply supported beam with the length $l_\mathrm{A} = \sqrt{\pi}$ [m], the eigenmodes up to the 8th, 16th, and 32nd orders, which correspond to 80 % of them, were used. This is because these natural frequencies can be obtained with sufficient precision, which is discussed in Section 3.3.

3.2 Verification of the line density and bending stiffness of the elimination region

In this section, the simulation results are presented for small values of the line density and bending stiffness of the elimination regions. The condition number of the matrix is improved because of the small values. However, the elimination regions have mechanical impedance. This affects the precision of the natural frequencies and deteriorates the precision of the simulation results. The two boundary conditions and two beams described in Section 3.1 were used in these simulations, and the magnitude of the error rate of the first-order natural frequency was evaluated.

The material properties of region A used in the simulations to verify the line density and bending stiffness of the elimination regions were identical to those listed in Table 1. The highest-order n of the eigenmode was 20 in these simulations. The simulation results for the magnitude of the error rate of the first-order natural frequency are shown in Fig. 3. The line density ratio A_μ and bending stiffness ratio A_D are defined using the following equations:

$$A_\mu = \frac{\mu_\mathrm{B}}{\mu_\mathrm{A}} = \frac{\mu_\mathrm{C}}{\mu_\mathrm{A}}, \quad A_D = \frac{D_\mathrm{B}}{D_\mathrm{A}} = \frac{D_\mathrm{C}}{D_\mathrm{A}}. \tag{37}$$

$\mu_\mathrm{B} = \mu_\mathrm{C}$ and $D_\mathrm{B} = D_\mathrm{C}$ were used in these simulations. In addition, $A_\mu = A_D$ was used. From Fig. 3, it can be seen that the small values of the line density and bending stiffness reduced the condition number problem as expected. When $A_\mu\,(= A_D)$ is large, the magnitude of the error rate takes values close to those of $A_\mu\,(= A_D)$. These are natural results, and when small values are used, $A_\mu\,(= A_D)$ can be used to estimate precision. However, the regions in which the simulation results are better than those of $A_\mu = A_D = 0$ are limited to regions in which A_λ is large and $A_\mu\,(= A_D)$ is small. Therefore, $A_\mu = A_D = 0$ can be used if A_λ is appropriately selected. In Fig. 3, the simulation results of the error rate have several local minimums. The local minimums at $A_\lambda = 2.5$ occur because the translational or rotational mechanical impedances of the elimination regions at the first-order natural frequency are zero. Preferably, the translational and rotational mechanical impedances of the elimination region should be zero when the new boundary is a guided and supported end, respectively. In Fig. 3(a), there are several local minimums at points other than $A_\lambda = 2.5$ when the guided-guided beam was used as the original beam. When $A_\lambda = 1$ and 1.5, $l_\mathrm{B} = l_\mathrm{C} = \lambda_{20}$ and $1.5\lambda_{20}$, respectively. Therefore, the slope of the highest nth-order eigenmode for $x = x_\mathrm{B}$ and x_C was zero in these cases. This

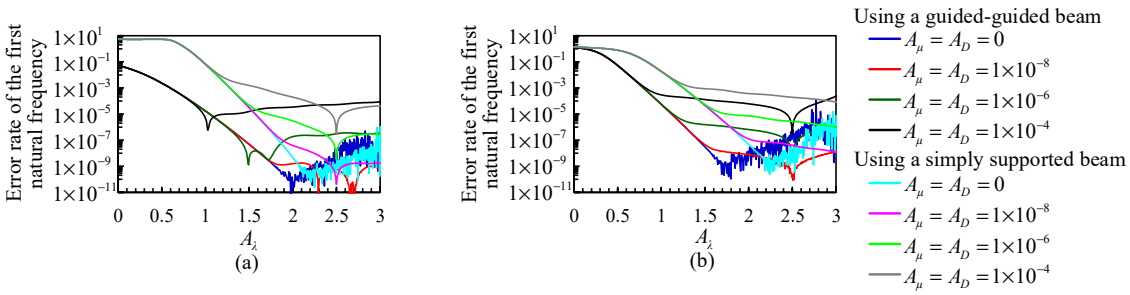

Fig. 3 Simulation results of the magnitude of the error rate of the first natural frequency obtained through the substructure elimination method wherein the line densities and bending stiffnesses have small values: (a) case where guided ends were set on the new boundaries, and (b) case where supported ends were set on the new boundaries.

[DOI: 10.1299/mej.23-00293]
© 2023 The Japan Society of Mechanical Engineers

is advantageous for setting a new boundary with zero slope at $x = x_B$ and $x = x_C$. Although the graphs are not presented, A_λ at which the local minimums appear also depends on A_μ, and the effect of A_D is small. Therefore, the condition for the occurrence of these local minimums also depends on the mass and moment of inertia of the elimination regions. Thus, utilizing these local minimums in simulations is not recommended because the condition for the occurrence of the local minimums varies depending on the type of new boundaries. When the condition number problem is more likely to occur than the authors' simulation environment, small values of A_μ and A_D should be used to improve this problem.

3.3 Verification to determine the highest order of the eigenmode of the original beam

The frequency range in which the natural frequencies can be obtained with a high precision depends on the natural frequency of the highest *n*th-order eigenmode of the original beam. Simulations were conducted to investigate this frequency range. The two boundary conditions and two beams described in Section 3.1 were used in these simulations. The material properties used in the simulations are listed in Table 2. The natural frequencies of the original beams were obtained using the product of $16/49 \approx 0.33$ Hz and square of the natural numbers. Therefore, the natural frequency of the highest 14th-order eigenmode of the original beams was 64 Hz. The natural frequencies obtained using MATLAB's eigenvalue analysis are listed in Table 3. In all cases, natural frequencies of 0 Hz were omitted, as shown in Table 3. Natural frequencies of 0 Hz owing to the zeroth-order eigenmode of the original beams were obtained when the equation of motion for the eigenmode was not coupled with those of other eigenmodes. When the guided ends were set at both of the new boundaries, a translational rigid body mode was obtained. In addition to these natural frequencies of 0 Hz, two additional natural frequencies of 0 Hz were obtained in all cases, and their number was equal to that of the acceleration constraints. When the clamped ends were set at both of the new boundaries, four additional natural frequencies of 0 Hz were obtained rather than two. This is because the translational and rotational acceleration constraints contribute to the large mass and moment of inertia, respectively. Similar results are obtained when a large mass and moment of inertia are installed at the new boundaries. When the displacement constraints are set or translational and rotational stiff springs are

Table 2 Material properties used in the verification simulations to determine the highest order of the eigenmode of the original beam.

μ_A	0.2 kg/m	$\mu_B = \mu_C$	0 kg/m
D_A	0.8 Nm^2	$D_B = D_C$	0 Nm^2
l_A	$\sqrt{\pi} \approx 1.772$ m	$l_B = l_C$	$3l_A/8$ m
A_λ	1.5	n	14

Table 3 Natural frequencies obtained using MATLAB's eigenvalue analysis. The natural frequency of the highest *n*th-order eigenmode of the original beam was 64 Hz in these simulations.

New boundaries	Set to guided ends		Set to supported ends	
Original beam	Guided-guided beam	Simply supported beam	Guided-guided beam	Simply supported beam
Exact natural frequencies [Hz]	Calculated natural frequencies [Hz]			
1	1.000000032	1.000000590	1.000000001	1.000012048
4	4.000000007	4.000002651	4.000000028	4.000000736
9	9.000000017	9.000001068	9.000000023	9.000000693
16	16.00000007	16.00000000	16.00000000	16.00000181
25	25.00000021	25.00000355	25.00000023	25.00000281
36	36.00000077	36.00004444	36.00000514	36.00000792
49	49.00013631	49.00001666	49.00000238	49.00078252
64	64.00000000	64.05129392	64.01344566	64.00000000
81	81.93378613	81.27977082	81.08530525	83.56815544
100	102.2211972	124.8794206	110.1024828	105.5977924
121	178.8071445	161.7701573	138.3314756	282.9540437
144	229.037135	-	440.1237117	377.6733907
169	-	-	572.1687745	-

[DOI: 10.1299/mej.23-00293]
© 2023 The Japan Society of Mechanical Engineers

installed at the new boundaries, these additional natural frequencies of 0 Hz are not obtained. In these cases, the same number of significantly large natural frequencies are obtained rather than the natural frequencies of 0 Hz. These eigenmodes did not cause inaccuracies in the frequency response functions. The frequency response functions are presented in Section 3.4. The natural frequencies are listed in 10 digits in Table 3. Because $A_\lambda = 1.5$ was used in these simulations, the guided-guided beam is superior to the simply supported beam in terms of precision. However, the simulation results for the simply supported beam were also sufficiently precise in terms of practical use. The several simulation results for the fourth- and eighth-order eigenmodes have no error. This is because the seventh- and 14th-order eigenmodes of the original beams can be directly used for the generated fourth- and eighth-order eigenmodes, respectively. Ignoring these special cases, the precision of the natural frequencies significantly varied at 64 Hz. Therefore, the frequency range in which the natural frequencies can be obtained with a high precision is less than that of the highest *n*th-order eigenmode of the original beams. When the frequency range is limited to a higher precision, the upper limit of the frequency range should be lower than the highest *n*th-order natural frequency. The simulation results listed in Table 3 confirm that there is no significant difference in the error rates between using multiple natural frequencies and using only the first-order natural frequency in Fig. 2.

In the simulation using the substructure elimination method, the elimination length $l_B = l_C$ and highest-order n of the eigenmode of the original beams should be determined. The natural frequency of the highest *n*th-order eigenmode depends on both $l_B = l_C$ and n. Therefore, the natural frequency of the highest *n*th-order eigenmode is tentatively defined as $f_{n\mathrm{T}}$. The tentative natural frequency $f_{n\mathrm{T}}$ and elimination length $l_B = l_C$ are expressed as

$$f_{n\mathrm{T}} = \frac{1}{2\pi}\left(\frac{n\pi}{l_{\mathrm{ABC}}}\right)^2\sqrt{\frac{D_\mathrm{A}}{\mu_\mathrm{A}}},\quad l_\mathrm{B} = l_\mathrm{C} = A_{\lambda\mathrm{T}}\lambda_n, \tag{38}$$

respectively, where $A_{\lambda\mathrm{T}}$ is the tentative number of wavelengths. Because l_A and $\sqrt{D_\mathrm{A}/\mu_\mathrm{A}}$ are provided, and $A_{\lambda\mathrm{T}}$ and $f_{n\mathrm{T}}$ are arbitrarily determined by the user, the elimination length $l_B = l_C$ can be derived from Eqs. (36) and (38) as

$$l_\mathrm{B} = l_\mathrm{C} = A_{\lambda\mathrm{T}}\sqrt{\frac{2\pi}{f_{n\mathrm{T}}}}\sqrt[4]{\frac{D_\mathrm{A}}{\mu_\mathrm{A}}}. \tag{39}$$

Using Eqs. (36) and (39), the highest-order n can be derived as

$$n = \left\lceil \frac{l_\mathrm{A}}{\pi}\sqrt{2\pi f_{n\mathrm{T}}}\sqrt[4]{\frac{\mu_\mathrm{A}}{D_\mathrm{A}}} + 4A_{\lambda\mathrm{T}} \right\rceil, \tag{40}$$

where the ceiling function was used to make n an integer. Because the elimination length $l_B = l_C$ and highest-order n are determined using Eqs. (39) and (40), respectively, the true natural frequency of the highest *n*th-order eigenmode and true number of wavelengths are expressed as

$$f_n = f_{n\mathrm{T}}\left(\frac{\left\lceil \frac{l_\mathrm{A}}{\pi}\sqrt{2\pi f_{n\mathrm{T}}}\sqrt[4]{\frac{\mu_\mathrm{A}}{D_\mathrm{A}}} + 4A_{\lambda\mathrm{T}} \right\rceil}{\frac{l_\mathrm{A}}{\pi}\sqrt{2\pi f_{n\mathrm{T}}}\sqrt[4]{\frac{\mu_\mathrm{A}}{D_\mathrm{A}}} + 4A_{\lambda\mathrm{T}}}\right)^2,\quad A_\lambda = A_{\lambda\mathrm{T}}\frac{\left\lceil \frac{l_\mathrm{A}}{\pi}\sqrt{2\pi f_{n\mathrm{T}}}\sqrt[4]{\frac{\mu_\mathrm{A}}{D_\mathrm{A}}} + 4A_{\lambda\mathrm{T}} \right\rceil}{\frac{l_\mathrm{A}}{\pi}\sqrt{2\pi f_{n\mathrm{T}}}\sqrt[4]{\frac{\mu_\mathrm{A}}{D_\mathrm{A}}} + 4A_{\lambda\mathrm{T}}}. \tag{41}$$

Because of the rounding off of n in Eq. (40), f_n and A_λ are marginally higher than $f_{n\mathrm{T}}$ and $A_{\lambda\mathrm{T}}$, respectively.

3.4 Verification using frequency response function

The effectiveness of the formulation of the guided and supported ends on the new boundaries was verified through the simulation results presented in Sections 3.1 to 3.3. In this section, the effectiveness of the formulation of the clamped end, free end, displacement excitation, and angular displacement excitation, and installation of the translational and rotational 1-DOF vibration systems at the new boundaries, is verified by comparing the simulation results of the substructure elimination method with exact solutions. Therefore, the cases in which exact solutions can be derived was considered. The following three beams were used: a beam subjected to a displacement and angular displacement

[DOI: 10.1299/mej.23-00293]
© 2023 The Japan Society of Mechanical Engineers

excitation at the new left boundary and clamped at the new right boundary, a beam which is free at the new left boundary and subjected to a displacement and angular displacement excitation at the new right boundary, and a beam with translational and rotational 1-DOF vibration systems at the new boundaries and external force and bending moment at the center of the beam. To obtain exact solutions for the third beam, completely identical 1-DOF vibration systems were installed at the new left and right boundaries. When the 1-DOF vibration systems were installed at the new boundaries, the simulations using the conventional modal analysis and a free-free beam were also conducted. The derivations for the exact solutions and conventional modal analysis using a free-free beam are also briefly described using the third beam as a representative.

3.4.1 Analytical model for the beam with 1-DOF vibration systems

The analytical models used in the simulation of the beam with 1-DOF vibration systems at the new left and right boundaries are shown in Fig. 4. Here, l_{Ah}, f_{exh}, and N_{exh} are halves of l_{A}, f_{ex}, and N_{ex}, respectively. The analytical model shown in Fig. 4(a) was used for conventional modal analysis using a free-free beam, and that shown in Fig. 4(b) was used for the derivation of the exact solutions. Because the analytical model shown in Fig. 4(a) is symmetrical with respect to the midpoint of the beam, only the right half of the beam in Fig. 4(b) is considered. When a beam is excited only by an external force, it vibrates line symmetrically about the midpoint, and when it is excited only by a bending moment, it vibrates point symmetrically. The symbols used in these analytical models are similar to those used in the analytical model shown in Fig. 1. The left ends of the beam were set to the origins of the x_{cm}- and x_{ex}-coordinates in the analytical models, as shown in Fig. 4(a) and (b), respectively, and the right-hand direction is the positive direction of these coordinates. In the analytical model shown in Fig. 1, the new left boundary is located at $x = x_{\mathrm{B}}$. Therefore, the relationship between x and x_{cm} is expressed as $x = x_{\mathrm{cm}} + x_{\mathrm{B}}$. In addition, the relationship between x and x_{ex} is expressed as $x = x_{\mathrm{ex}} + x_{\mathrm{B}} + l_{\mathrm{A}}/2$. The material properties of the beam used in these simulations are listed in Table 4. Here, W^{R}, Θ^{R}, $F_{\mathrm{ex}}^{\mathrm{R}}$, and $N_{\mathrm{ex}}^{\mathrm{R}}$ are the real amplitudes of w_{L} or w_{R}, θ_{L} or θ_{R}, f_{ex}, and N_{ex}, respectively. As listed in Table 4, the natural frequency of the highest *n*th-order eigenmode for the substructure elimination method was approximately 1030 Hz. Because the highest order of the eigenmode for the conventional modal analysis using a free-free beam was the 21st, the natural frequency of the highest *n*th-order eigenmode for the conventional method was approximately 2130 Hz. The phase differences between the displacement and angular displacement excitations and between the external force and bending moment were set to zero in these simulations. The material properties of the 1-DOF vibration systems are listed in Table 5. Here, j is the imaginary unit, Z_{T} and Z_{R} are the translational and rotational characteristic impedances of the beam, respectively, and they are expressed as

$$Z_{\mathrm{T}} = \sqrt{\mu_{\mathrm{A}} D_{\mathrm{A}}} \sqrt[4]{\frac{\mu_{\mathrm{A}}}{D_{\mathrm{A}}}} \sqrt{\omega}, \quad Z_{\mathrm{R}} = \frac{\sqrt{\mu_{\mathrm{A}} D_{\mathrm{A}}}}{\sqrt[4]{\frac{\mu_{\mathrm{A}}}{D_{\mathrm{A}}}} \sqrt{\omega}}, \tag{42}$$

where ω is the excitation angular frequency. Three material properties were used in the 1-DOF vibration systems, and all the material properties for Case (2) were 100 times larger than those for Case (1). In Cases (1) and (2), the undamped natural frequencies of the translational and rotational 1-DOF vibration systems were approximately 252 and 503 Hz, respectively, and their damping ratios were approximately 0.0949 and 0.0791, respectively. In these cases, the eigenvalue

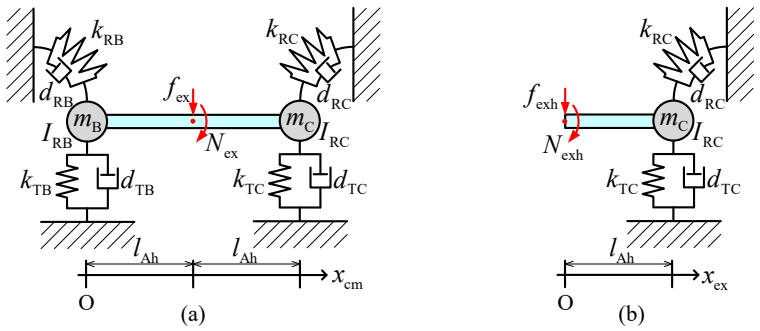

Fig. 4 Analytical models for conventional modal analysis using a free-free beam and the derivation of the exact solutions: (a) analytical model for the conventional modal analysis and (b) analytical model for derivation of the exact solutions.

[DOI: 10.1299/mej.23-00293]
© 2023 The Japan Society of Mechanical Engineers

Table 4 Material properties of the beam used in the simulations for obtaining the frequency response function.

ρ_{A}	2700 kg/m^3	$\rho_{\mathrm{B}} = \rho_{\mathrm{C}}$	0 kg/m^3
E_{A}	70 GPa	$E_{\mathrm{B}} = E_{\mathrm{C}}$	0 GPa
l_{A}	1 m	$f_{n\mathrm{T}}$	1000 Hz
b_{A}	50 mm	f_n	1028 Hz
t_{A}	2 mm	$A_{z\mathrm{T}}$	1.5
n	21	A_z	1.521
W^{R}	1 mm	$F_{\mathrm{ex}}^{\mathrm{R}}$	3 N
Θ^{R}	0.01 rad	$N_{\mathrm{ex}}^{\mathrm{R}}$	0.1 N m

Table 5 Material properties of the translational and rotational 1-DOF vibration systems used in the simulations to obtain the frequency response function.

	Case (1)	Case (2)	Case (3)
$m_{\mathrm{B}} = m_{\mathrm{C}}$ [g]	2	200	0
$d_{\mathrm{TB}} = d_{\mathrm{TC}}$ [N s/m]	0.6	60	0
$k_{\mathrm{TB}} = k_{\mathrm{TC}}$ [N/m]	5000	500000	$\mathrm{j}\omega Z_{\mathrm{T}}$
$I_{\mathrm{RB}} = I_{\mathrm{RC}}$ [kg m^2]	1×10^{-6}	1×10^{-4}	0
$d_{\mathrm{RB}} = d_{\mathrm{RC}}$ [N m s/rad]	5×10^{-4}	5×10^{-2}	0
$k_{\mathrm{RB}} = k_{\mathrm{RC}}$ [N m/rad]	10	1000	$\mathrm{j}\omega Z_{\mathrm{R}}$

analysis was performed after deriving the equation of state. In Case (3), only the translational and rotational spring constants with pure imaginary numbers were applied to convert new boundaries into non-reflective boundaries (Iwaya et al., 2000; Oberst et al., 2021). Specifically, these were non-vibration systems because they did not have natural frequencies. In this case, an eigenvalue analysis was performed using the equations of motion rather than the equation of state. The translational and rotational impedances of the translational and rotational spring constants for Case (3) were equal to the translational and rotational characteristic impedances of the beam. The material properties for Case (1) and (2) were those that result in impedances less and larger than the characteristic impedances in most of the targeted frequency regions, respectively. Because the characteristic impedances of the beam depend on the frequency, the simulations for Case (3) were performed using difference spring constants for each excitation frequency. It only took a few seconds to calculate the excitation frequency of 600 points on a personal computer with an Intel Core i7-8565U CPU.

3.4.2 Derivation of the exact solution using boundary conditions

The equation of motion of the minute fraction of the analytical model shown in Fig. 4(b) is expressed as

$$\mu_{\mathrm{A}} \frac{\partial^2 w}{\partial t^2} + D_{\mathrm{A}} \frac{\partial^4 w}{\partial x_{\mathrm{ex}}^4} = 0 \,. \tag{43}$$

When obtaining exact solutions using boundary conditions, the terms of the external force and bending moment are not included in the equation of motion. From Eq. (43), the deflection $w(x_{\mathrm{ex}}, t)$ is derived as

$$w(x_{\mathrm{ex}}, t) = W(x_{\mathrm{ex}})\mathrm{e}^{\mathrm{j}\omega t}\,,\quad W(x_{\mathrm{ex}}) = C_1\cos kx_{\mathrm{ex}} + C_2\sin kx_{\mathrm{ex}} + C_3\cosh kx_{\mathrm{ex}} + C_4\sinh kx_{\mathrm{ex}}\,,\quad k = \sqrt[4]{\frac{\mu_{\mathrm{A}}}{D_{\mathrm{A}}}}\sqrt{\omega}\,, \tag{44}$$

where k is the wave number, and C_1, C_2, C_3, and C_4 are constants determined using the boundary conditions. The deflection expressed using Eq. (44) satisfies Eq. (43). Because the exact solution has hyperbolic function terms, correct numerical results cannot be obtained in high frequency regions.

The boundary conditions for the analytical model shown in Fig. 4(b) are obtained using

$$-D_{\mathrm{A}}\left.\frac{\partial^3 w}{\partial x_{\mathrm{ex}}^3}\right|_{x_{\mathrm{ex}}=0} = -f_{\mathrm{exh}}\,,\quad -D_{\mathrm{A}}\left.\frac{\partial^2 w}{\partial x_{\mathrm{ex}}^2}\right|_{x_{\mathrm{ex}}=0} = N_{\mathrm{exh}}\,,\quad -D_{\mathrm{A}}\left.\frac{\partial^3 w}{\partial x_{\mathrm{ex}}^3}\right|_{x_{\mathrm{ex}}=l_{\mathrm{Ah}}} = -m_{\mathrm{C}}\left.\ddot{w}\right|_{x_{\mathrm{ex}}=l_{\mathrm{Ah}}} - d_{\mathrm{TC}}\left.\dot{w}\right|_{x_{\mathrm{ex}}=l_{\mathrm{Ah}}} - k_{\mathrm{TC}}\left.w\right|_{x_{\mathrm{ex}}=l_{\mathrm{Ah}}}\,, \tag{45}$$

[DOI: 10.1299/mej.23-00293]
© 2023 The Japan Society of Mechanical Engineers

$$-D_{\mathrm{A}}\left.\frac{\partial^2 w}{\partial x_{\mathrm{ex}}^2}\right|_{x_{\mathrm{ex}}=l_{\mathrm{Ah}}}=I_{\mathrm{RC}}\left.\frac{\partial^3 w}{\partial x_{\mathrm{ex}}\partial t^2}\right|_{x_{\mathrm{ex}}=l_{\mathrm{Ah}}}+d_{\mathrm{RC}}\left.\frac{\partial^2 w}{\partial x_{\mathrm{ex}}\partial t}\right|_{x_{\mathrm{ex}}=l_{\mathrm{Ah}}}+k_{\mathrm{RC}}\left.\frac{\partial w}{\partial x_{\mathrm{ex}}}\right|_{x_{\mathrm{ex}}=l_{\mathrm{Ah}}}. \tag{46}$$

Using Eqs. (45) and (46), C_1, C_2, C_3, and C_4 are obtained, and exact solutions for the deflection, slope, bending moment, and shear force can be derived. The exact solutions for the other boundary conditions can also be derived using the same procedure.

3.4.3 Conventional modal analysis using a free-free beam

The equation of motion of the minute fraction for the analytical model shown in Fig. 4(a) is expressed as

$$\mu_{\mathrm{A}}\frac{\partial^2 w}{\partial t^2}+D_{\mathrm{A}}\frac{\partial^4 w}{\partial x_{\mathrm{cm}}^4}=f_{\mathrm{B}}\delta(x_{\mathrm{cm}})-N_{\mathrm{B}}\delta'(x_{\mathrm{cm}})+f_{\mathrm{C}}\delta(x_{\mathrm{cm}}-l_{\mathrm{A}})-N_{\mathrm{C}}\delta'(x_{\mathrm{cm}}-l_{\mathrm{A}})+f_{\mathrm{ex}}\delta(x_{\mathrm{cm}}-l_{\mathrm{Ah}})-N_{\mathrm{ex}}\delta'(x_{\mathrm{cm}}-l_{\mathrm{Ah}}), \tag{47}$$

$$f_{\mathrm{B}}=-m_{\mathrm{B}}\ddot{w}|_{x_{\mathrm{cm}}=0}-d_{\mathrm{TB}}\dot{w}|_{x_{\mathrm{cm}}=0}-k_{\mathrm{TB}}w|_{x_{\mathrm{cm}}=0},\quad N_{\mathrm{B}}=-I_{\mathrm{RB}}\left.\frac{\partial^3 w}{\partial x_{\mathrm{cm}}\partial t^2}\right|_{x_{\mathrm{cm}}=0}-d_{\mathrm{RB}}\left.\frac{\partial^2 w}{\partial x_{\mathrm{cm}}\partial t}\right|_{x_{\mathrm{cm}}=0}-k_{\mathrm{RB}}\left.\frac{\partial w}{\partial x_{\mathrm{cm}}}\right|_{x_{\mathrm{cm}}=0}, \tag{48}$$

$$f_{\mathrm{C}}=-m_{\mathrm{C}}\ddot{w}|_{x_{\mathrm{cm}}=l_{\mathrm{A}}}-d_{\mathrm{TC}}\dot{w}|_{x_{\mathrm{cm}}=l_{\mathrm{A}}}-k_{\mathrm{TC}}w|_{x_{\mathrm{cm}}=l_{\mathrm{A}}},\quad N_{\mathrm{C}}=-I_{\mathrm{RC}}\left.\frac{\partial^3 w}{\partial x_{\mathrm{cm}}\partial t^2}\right|_{x_{\mathrm{cm}}=l_{\mathrm{A}}}-d_{\mathrm{RC}}\left.\frac{\partial^2 w}{\partial x_{\mathrm{cm}}\partial t}\right|_{x_{\mathrm{cm}}=l_{\mathrm{A}}}-k_{\mathrm{RC}}\left.\frac{\partial w}{\partial x_{\mathrm{cm}}}\right|_{x_{\mathrm{cm}}=l_{\mathrm{A}}}. \tag{49}$$

When a free-free beam is used, the deflection w is expressed as

$$w(x_{\mathrm{cm}},t)=W_{0\mathrm{T}}(x_{\mathrm{cm}})\xi_{0\mathrm{T}}(t)+W_{0\mathrm{R}}(x_{\mathrm{cm}})\xi_{0\mathrm{R}}(t)+\sum_{h=1}^{n}W_h(x_{\mathrm{cm}})\xi_h(t), \tag{50}$$

$$W_{0\mathrm{T}}(x_{\mathrm{cm}})=A_{0\mathrm{T}},\quad W_{0\mathrm{R}}(x_{\mathrm{cm}})=A_{0\mathrm{R}}\left(x_{\mathrm{cm}}-\frac{l_{\mathrm{A}}}{2}\right), \tag{51}$$

$$W_h(x_{\mathrm{cm}})=A_{h\mathrm{cm}}\left[\cos k_{h\mathrm{cm}}x_{\mathrm{cm}}+\cosh k_{h\mathrm{cm}}x_{\mathrm{cm}}-\frac{\cos k_{h\mathrm{cm}}l_{\mathrm{A}}-\cosh k_{h\mathrm{cm}}l_{\mathrm{A}}}{\sin k_{h\mathrm{cm}}l_{\mathrm{A}}-\sinh k_{h\mathrm{cm}}l_{\mathrm{A}}}(\sin k_{h\mathrm{cm}}x_{\mathrm{cm}}+\sinh k_{h\mathrm{cm}}x_{\mathrm{cm}})\right], \tag{52}$$

where $W_{0\mathrm{T}}$, $W_{0\mathrm{R}}$, and W_h are the eigenfunctions of the deflection for the translational and rotational rigid body modes and bending vibration modes, respectively, $\xi_{0\mathrm{T}}$, $\xi_{0\mathrm{R}}$, and ξ_h are the modal displacements for these eigenmodes, $A_{0\mathrm{T}}$, $A_{0\mathrm{R}}$, and $A_{h\mathrm{cm}}$ are the arbitrary constants, and $k_{h\mathrm{cm}}$ is the wave number. The wave number $k_{h\mathrm{cm}}$ can be numerically obtained using the following frequency equation:

$$\cos k_{h\mathrm{cm}}l_{\mathrm{A}}\cosh k_{h\mathrm{cm}}l_{\mathrm{A}}-1=0. \tag{53}$$

In the simulations in this study, when h was seven or more, $k_{h\mathrm{cm}}l_{\mathrm{A}}$ was approximated using $k_{h\mathrm{cm}}l_{\mathrm{A}}=(h-1.5)\pi$. Moreover, all eigenfunctions are orthogonal, including in the rigid body modes. The equations of motion using modal displacements are obtained by substituting Eq. (50) into Eq. (47), multiplying both sides by the eigenfunctions, and integrating over the entire range of the beam. The modal masses can also be normalized to one by dividing both sides by μ_{A} and using $A_{0\mathrm{T}}=1/\sqrt{l_{\mathrm{A}}}$, $A_{0\mathrm{R}}=2\sqrt{3}/\left(l_{\mathrm{A}}\sqrt{l_{\mathrm{A}}}\right)$, and $A_{h\mathrm{cm}}=1/\sqrt{l_{\mathrm{A}}}$ when performing the integration. Two drawbacks of the conventional modal analysis using a free-free beam are that the algebraic solution for the frequency equation cannot be obtained, and the eigenfunction has hyperbolic terms.

3.4.4 Simulation results

Owing to page limitations, all simulation results cannot be presented in this study. Therefore, only the important and representative simulation results are presented.

The simulation results of the nondimensional deflection and bending moment at $x=x_{\mathrm{B}}+0.7l_{\mathrm{A}}$, which were obtained using a beam subjected to a displacement and angular displacement excitation at the new left boundary and clamped at the new right boundary, and a beam which is free at the new left boundary and subjected to a displacement and angular displacement excitation at the new right boundary, are presented in Figs. 5 and 6, respectively. Here, W^* and N^* are the complex amplitudes of w and N, respectively, and the frequency resolution was 2.5 Hz in these simulations. Owing to the frequency resolution, the peaks and anti-resonance points had finite values. Below $f_n\approx 1030$ [Hz], the simulation results of the substructure elimination method are in good agreement with the exact solutions. Above 1000 Hz, the results of the exact solutions are evidently inaccurate owing to the hyperbolic function. The simulation results of the

[DOI: 10.1299/mej.23-00293]
© 2023 The Japan Society of Mechanical Engineers

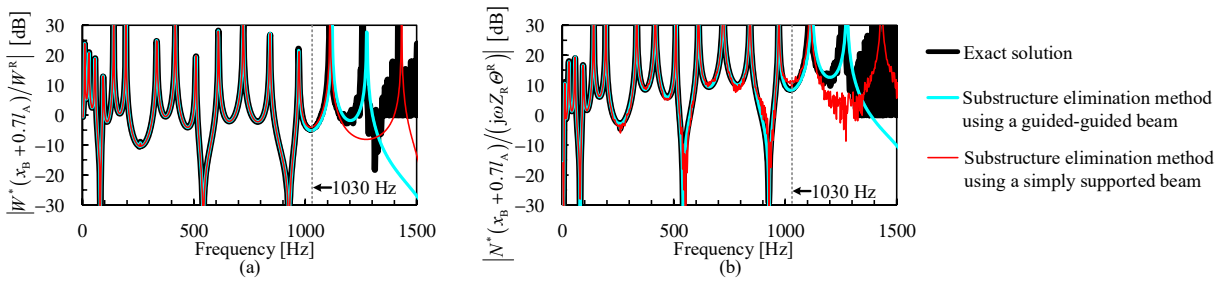

Fig. 5 Simulation results of the nondimensional deflection and bending moment at $x = x_B + 0.7l_A$, which were obtained using a beam subjected to a displacement and angular displacement excitation at the new left boundary and clamped at the new right boundary: (a) nondimensional deflection and (b) nondimensional bending moment.

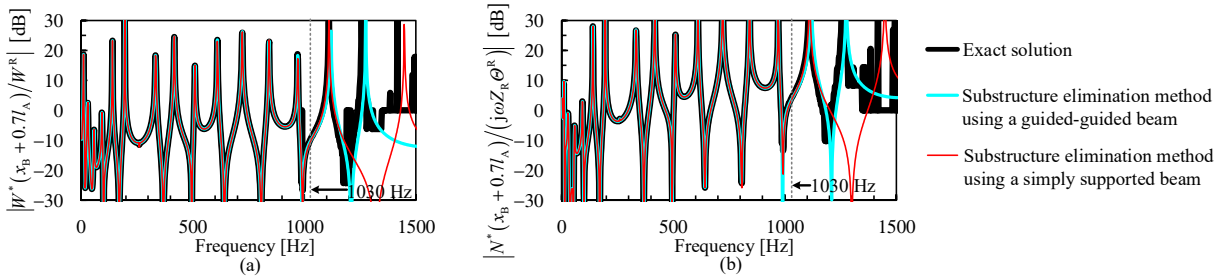

Fig. 6 Simulation results of the nondimensional deflection and bending moment at $x = x_B + 0.7l_A$, which were obtained using a beam that is free at the new left boundary and subjected to a displacement and angular displacement excitation at the new right boundary: (a) nondimensional deflection and (b) nondimensional bending moment.

bending moment of the simply supported beam was inaccurate in the frequency region with small vibrations, as shown in Fig. 5(b). This is owing to the fact that Eq. (35) is more affected by low-order eigenmodes than Eq. (30). The number of significant digits was insufficient. Although the additional simulation result was omitted in Fig. 5(b) to avoid overlapping graphs, this problem improves with an increase in the number of eigenmodes, and was solved by increasing $n = 21$ to 30. The simulation results for the slope and shear force also agreed well with the exact solutions below $f_n \approx 1030$ [Hz], although they were also omitted here. In the simulations with excitation at the new boundaries, the simulation results of the substructure elimination method agreed well with the exact solution even at the coordinates near the boundaries, although these results are not presented herein. In principle, it seems unnecessary to eliminate regions B and C when a beam subjected to a displacement and angular displacement excitation at the new left boundary and clamped at the new right boundary because the beam is constrained at the new boundaries. However, when the same linear density and bending stiffness in region A were applied to regions B and C, the simulation results did not agree with the exact solutions above 100 Hz. This is because deflection values cannot be freely taken in regions B and C if they are not eliminated.

The simulation results of the nondimensional deflection, slope, bending moment, and shear force at $x = x_B + 0.5l_A$, which were obtained using a beam with translational and rotational 1-DOF vibration systems at the new boundaries and external force and bending moment at the center of the beam, are presented in Fig. 7. Here, Θ^* and F_S^* are the complex amplitudes of θ and f_S, respectively. The material properties of Case (1), which are listed in Table 5, were used for the 1-DOF vibration systems. The simulation results obtained using the substructure elimination method are better than those obtained using the conventional modal analysis with a free-free beam. Below $f_n \approx 1030$ [Hz], the simulation results of the substructure elimination method agree well with the exact solutions, particularly near the resonance peaks. The simulation results for the deflection obtained using the substructure elimination method are slightly different from the exact solution near the anti-resonance points that are close to $f_n \approx 1030$ [Hz]. This is owing to the effect of the shear force and bending moment discontinuities at the excitation point. When the precision in the frequency region wherein vibration is small needs to be improved, n should be increased. For example, if the precision of the anti-resonance point around 500 Hz is sufficient, f_{nT} should be doubled. In this case, n increases from 21 to 27, and $f_n \approx 2030$ [Hz]. The effect of the higher-order eigenmodes is relatively large at the coordinates near the excitation point.

The simulation results of the nondimensional deflection and shear force at $x = x_B + 0.5l_A$, which were obtained using the material properties of Case (2), are presented in Fig. 8. Here, the simulation results of the slope and bending

[DOI: 10.1299/mej.23-00293]
© 2023 The Japan Society of Mechanical Engineers

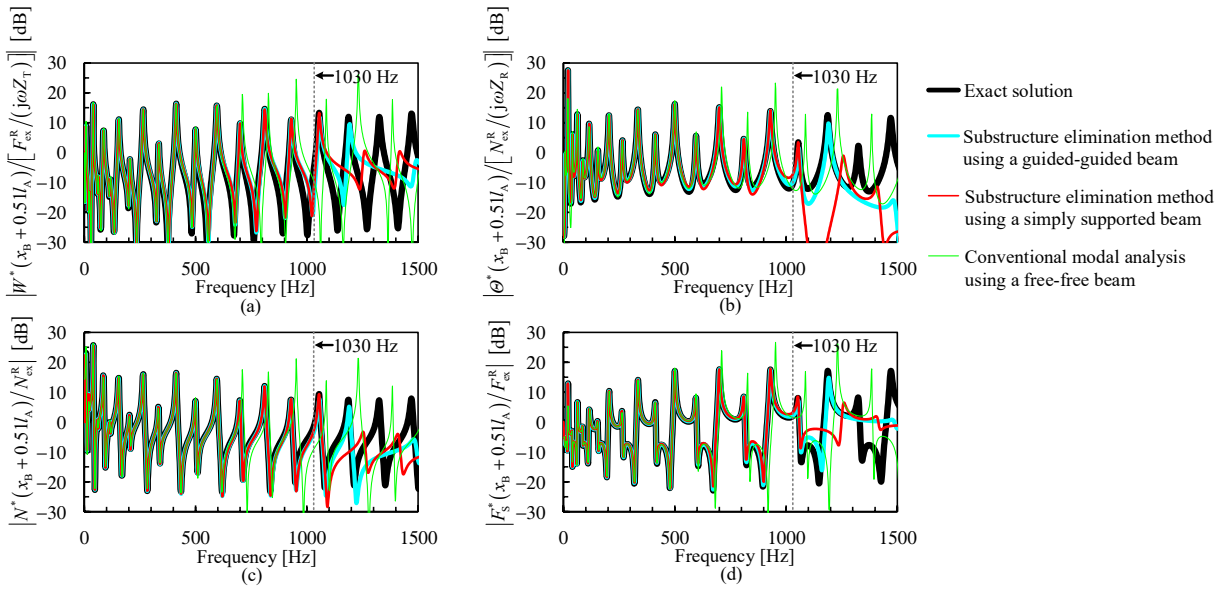

Fig. 7 Simulation results of the nondimensional deflection, slope, bending moment and shear force at $x = x_B + 0.5l_A$ when the material properties of Case (1), listed in Table 5, were used: (a) nondimensional deflection, (b) nondimensional slope, (c) nondimensional bending moment and (d) nondimensional shear force.

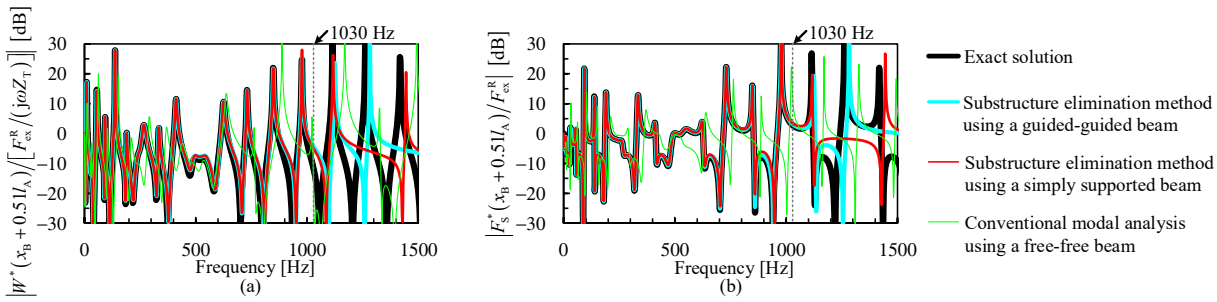

Fig. 8 Simulation results of the nondimensional deflection and shear force at $x = x_B + 0.5l_A$ when the material properties of Case (2), listed in Table 5, were used: (a) nondimensional deflection and (b) nondimensional shear force.

moment were omitted because they did not have special features. In this case, the precision of the conventional modal analysis deteriorated compared to the simulation results obtained using the material properties of Case (1). This is because the mode shapes were modified by the 1-DOF vibration systems installed at the new boundaries. The tendency of the simulation results using the substructure elimination method is not much different from that obtained using the material properties of Case (1). The substructure elimination method is more advantageous than the conventional modal analysis with a free-free beam when the impedances of the 1-DOF vibration systems are large. In the substructure elimination method, the superposition of eigenmodes is mainly Fourier cosine and sine series. It can be said that these series are superior to the superposition of the eigenmodes of a free-free beam.

The simulation results of the nondimensional deflection and shear force at $x = x_B + 0.5l_A$, which were obtained using the material properties of Case (3), are presented in Fig. 9. Here, the simulation results of the slope and bending moment were omitted because they did not have special features. The simulation results of the conventional modal analysis were inaccurate because both ends were non-reflective boundaries, and the vibration was significantly different from the standing wave generated in a free-free beam. The substructure elimination method is more advantageous than the conventional modal analysis with a free-free beam. However, particularly for deflection, a difference was observed between the exact solution and simulation results of the substructure elimination method, even below $f_n \approx 1030$ [Hz]. This is the same reason why there was a difference near the anti-resonance points when the material properties of Case (1) were used. To reduce the difference, $f_{n\mathrm{T}}$ should be set higher. The simulation results of the nondimensional deflection at $x = x_B + 0.5l_A$, which were obtained by increasing $f_{n\mathrm{T}}$ from 1000 Hz to 10000 Hz, are presented in Fig. 10(a). In this case, n was increased from 21 to 53. In addition, the simulation results of the nondimensional deflection at $x = x_B + 0.7l_A$, which were obtained without increasing $f_{n\mathrm{T}}$, are presented in Fig. 10(b). The precision of the simulation

[DOI: 10.1299/mej.23-00293]
© 2023 The Japan Society of Mechanical Engineers

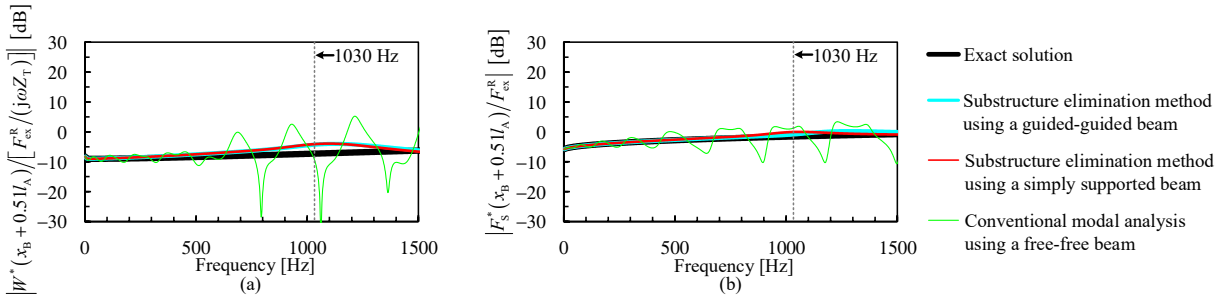

Fig. 9 Simulation results of the nondimensional deflection and shear force at $x = x_B + 0.51l_A$ when the material properties of Case (3), listed in Table 5, were used: (a) nondimensional deflection and (b) nondimensional shear force.

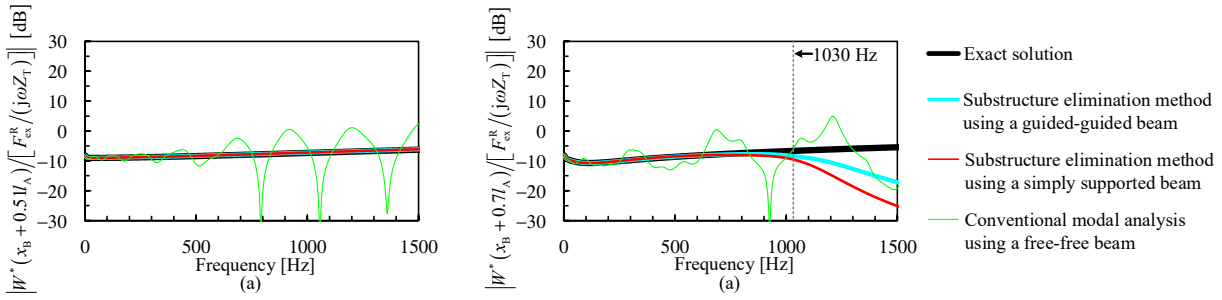

Fig. 10 Simulation results of the nondimensional deflection when $f_{nT} = 10000\,[\mathrm{Hz}]$ and $x = x_B + 0.7l_A$ were used rather than $f_{nT} = 1000\,[\mathrm{Hz}]$ and $x = x_B + 0.51l_A$, respectively: (a) case where $f_{nT} = 10000\,[\mathrm{Hz}]$ was used rather than $f_{nT} = 1000\,[\mathrm{Hz}]$ and (b) case where $x = x_B + 0.7l_A$ was used rather than $x = x_B + 0.51l_A$.

results increases as the number of eigenmodes increases, and the effect of the higher-order eigenmodes becomes relatively smaller as the distance from the excitation point increases.

The comparison of the frequency response functions indicates no significant difference between using the guided-guided beam and simply supported beam as the original beam.

4. Conclusion

In this study, the substructure elimination method for a beam was described. In addition to a guide-guided beam, the substructure elimination method using a simply supported beam as an original beam was also proposed. Based on constraint conditions, new formulations were proposed for setting arbitrary boundary conditions for new boundaries. The formulations for installing a free end, simply supported end, guided end, clamped end, displacement and angular displacement excitations, and arbitrary mechanical impedances using translational and rotational 1-DOF vibration systems on a new boundary, were elaborated. The following knowledge was obtained through the investigation using simulations: the line density and bending stiffness of the elimination regions should be zero if the deterioration of the matrix condition number is not problematic. The length of the elimination region should be set to 1.5–2.5 times the wavelength of the highest eigenmode when the eigenvalue analysis is performed as a standard eigenvalue problem using an inverse matrix of the mass matrix in the MATLAB simulations. For an equal number of eigenmodes, shorter elimination regions cover higher frequencies with high accuracy because the natural frequencies of the original beam are higher. In this study, formulations for determining the lengths of the elimination regions and highest-order of the eigenmode were derived based on the upper limit of the frequency range. Consequently, modal analysis using the substructure elimination method was found to be more advantageous than conventional modal analysis using a free-free beam.

Acknowledgment

This work was partially supported by a Grant-in-Aid for Scientific Research (C) (JSPS KAKENHI Grant Number JP21K03956) and financially supported partially by the Kansai University Fund for Domestic and Overseas Research Fund, 2022. This research was conducted while the first author stayed at the University of Technology Sydney as a

 © 2023 The Japan Society of Mechanical Engineers

visiting professor. The authors are grateful to the university for this appointment.

References

Benaroya, H. and Nagurka, M. L., Mechanical Vibration: Analysis, Uncertainties, and Control, Third edition (2009), CRC Press.

Bishop, R. E. D. and Johnson, D. C., The Mechanics of Vibration (1960), Cambridge University Press.

Iwaya, Y., Suzuki, Y., Sakata, M., and Sone, T., Influence of the terminating impedance of a semi-infinite beam on the reflection of bending wave and vibration intensity, Journal of the Acoustical Society of Japan, Vol. 56, No. 4(2000), pp. 243–248 (in Japanese).

Meirovitch, L., Analytical Methods in Vibrations (1967), Macmillan.

Meirovitch, L., Dynamics and Control of Structures (1990), John Wiley & Sons.

Meirovitch, L., Fundamentals of Vibrations (2001), McGraw-Hill Higher Education.

Nagamatsu, A., Modal Analysis (1985), Baifukan (in Japanese).

Oberst, S., Halkon, B., Ji, J. C, and Brown, T., Vibration Engineering for a Sustainable Future (2021), Springer, Cham, pp. 97–103.

Ohtomi, K., Kansei modeling for delight design based on 1DCAE concept, Proceedings of the 11th International Modelica Conference (2015), pp. 811–815.

Rao, S. S., Vibration of Continuous Systems (2007), John Wiley & Sons.

Reismann, H., Elastic Plates: Theory and Application (1988), John Wiley & Sons.

Shabana, A. A., Theory of Vibration: Volume II: Discrete and Continuous Systems (1991), Springer-Verlag New York, Inc.

Yamada, K., Proposal of substructure change or elimination method, Dynamics and Design Conference (2017), p. 440(12 pages) (in Japanese).

Yamada, K., Vibration analysis using substructure change and elimination methods, Proceedings of the 25th International Congress on Sound and Vibration (2018), p. 485(8 pages).

Yamada, K. and Ji, J. C., Substructure elimination method for vibration systems governed by a one-dimensional wave equation, Mechanical Engineering Journal, Vol. 10, No. 5(2023), DOI: 10.1299/mej.23-00241.

Yamada, K. and Asami, T., Passive vibration suppression using 2-degree-of-freedom vibration absorber consisting of a beam and piezoelectric elements, Journal of Sound and Vibration, Vol. 532, (2022), Article 116997, pp. 1–28.

Yamada, K. and Utsuno, H., Modal analysis of continuous systems by replacing displacement excitation with equivalent excitation force and fixed boundary, Mechanical Engineering Journal, Vol. 7, No. 4(2020), DOI: 10.1299/mej.20-00003.

[DOI: 10.1299/mej.23-00293]
© 2023 The Japan Society of Mechanical Engineers